INTERNATIONAL ATOMIC ENERGY AGENCY
UNITED NATIONS EDUCATIONAL, SCIENTIFIC AND CULTURAL ORGANIZATION
INTERNATIONAL CENTRE FOR THEORETICAL PHYSICS
I.C.T.P., P.O. BOX 586, 34100 TRIESTE, ITALY, CABLE: CENTRATOM TRIESTE

SMR.764 - 2

RESEARCH WORKSHOP ON CONDENSED MATTER PHYSICS
13 JUNE - 19 AUGUST 1994

MINIWORKSHOP ON "NONLINEAR TIME SERIES ANALYSIS" 8 - 12 AUGUST 1994

"Control of Chaotic Systems using Nonlinear Time Series"

Celso GREBOGI
Laboratory for Plasma & Fusion
University of Maryland
College Park, MD 20742
U.S.A.

Using small perturbations to control chaos

Troy Shinbrot, Celso Grebogi, Edward Ott & James A. Yorke

The extreme sensitivity of chaotic systems to tiny perturbations (the 'butterfly effect') can be used both to stabilize regular dynamic behaviours and to direct chaotic trajectories rapidly to a desired state. Incorporating chaos deliberately into practical systems therefore offers the possibility of achieving greater flexibility in their performance.

CHAOTIC systems are characterized by extreme sensitivity to tiny perturbations. This characteristic, known as the 'butterfly effect', is often regarded as a troublesome property, and for many years it has been generally believed that chaotic motions are neither predictable nor controllable. The first reference we find to a differing view is due to John von Neumann, who is reported[1] to have stated around 1950 that small, carefully chosen, pre-planned atmospheric disturbances could lead after some time to desired large-scale changes in the weather. Although this specific application might be problematic, the basic idea of using chaotic sensitivity seems to have been clearly appreciated by von Neumann. Here we review recent work which demonstrates that the butterfly effect permits the use of tiny feedback perturbations to control trajectories in chaotic systems—a capability without a counterpart in nonchaotic systems. These considerations apply to cases in which the chaotic dynamics can in principle be defined by only a few variables, so systems where there are many active degrees of freedom (for example, the weather, and high-Reynolds-number flows) may not be tractable. However, we emphasize that cases of high (or infinite) dimensional systems for which the 'attractor' (and hence the dynamics) is low dimensional are common.

The research that we will review fits broadly into two categories. First we will discuss how, as proposed in ref. 2, one can select a desired behaviour from among the infinite variety of behaviours naturally present in chaotic systems, and then stabilize this behaviour by applying only tiny changes to an accessible system parameter (related work appears in refs 3–32, 77, 78). Moreover, we will show how one can switch between behaviours as circumstances change, again using only tiny perturbations. This means that chaotic systems can achieve great flexibility in their ultimate performance. Second, we will show how one can use the sensitivity of chaotic systems to direct trajectories rapidly to a desired state[33–38]. For example, a few years ago, NASA scientists used only small amounts of residual hydrazine fuel to send the spacecraft ISEE-3/ICE more than 50 million miles across the Solar System, thereby achieving the first scientific cometary encounter[39–43]. This feat was made possible by the sensitivity of the three-body problem of celestial mechanics to small perturbations, and would not have been possible in a nonchaotic system, in which a large effect typically requires a large control[44–46].

Stabilizing unstable orbits

One of the fundamental aspects of chaos is that many different possible motions are simultaneously present in the system. A particular manifestation of this is the fact that there are typically an infinite number of unstable periodic orbits that co-exist with the chaotic motion[47,48]. By a periodic orbit, we mean an orbit that repeats itself after some time (the period). If the system were precisely on an unstable periodic orbit, it would remain on that orbit forever. These orbits are unstable in the sense that the smallest deviation from the periodic orbit (for example due to noise) grows exponentially rapidly in time, and the system orbit quickly moves away from the periodic orbit. Thus, although these periodic orbits are present, they are not typically observed. Rather, what one sees is a chaotic trajectory which bounces around in an erratic, seemingly random fashion. Very rarely, the chaotic trajectory may, by chance, closely approach a particular unstable periodic orbit, in which case the chaotic trajectory would approximately follow the periodic cycle for a few periods, but it would then rapidly move away because of the instability of the periodic orbit. In addition to periodic orbits, it is common for continuous time dynamical systems to have unstable steady states embedded in chaotic motion (see our subsequent discussion of the Lorenz attractor). A ball placed exactly at the top of a hill is an example of an unstable steady state.

Although the existence of steady states and an infinity of different unstable periodic orbits embedded in chaotic motion is not usually obvious in free-running chaotic evolution, these orbits offer a great potential advantage if one wants to control a chaotic system. To demonstrate this, we adopt the following strategy[2]. First we examine the unstable steady states and low-period unstable periodic orbits embedded in the chaotic motion. For each of those unstable orbits, we ask whether the system performance would be improved if that orbit were actually followed. We then select one of the unstable orbits that yields improved performance. Assuming the motion of the free-running chaotic orbit to be ergodic, eventually the chaotic wandering of an orbit trajectory will bring it close to the chosen unstable periodic orbit or steady state. When this occurs, we can apply our small controlling perturbations to direct the orbit to the desired periodic motion or steady state. Moreover, if a small amount of noise is present, we can repeatedly apply the perturba-

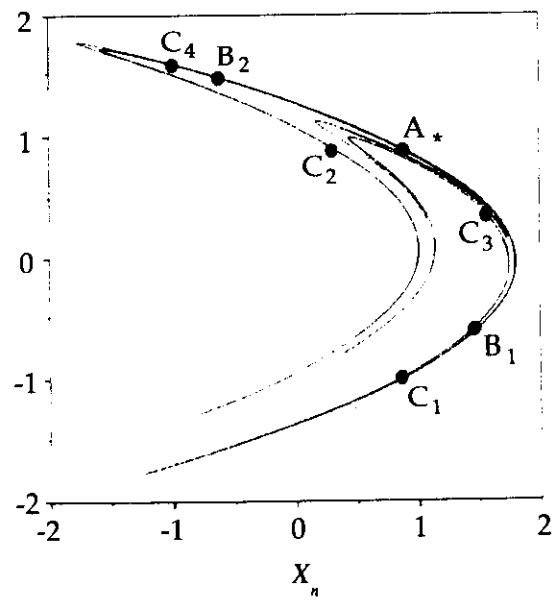

FIG. 1 Hénon attractor, with period-1 point, A_*; period-2 points, B_1 and B_2; and period-4 points, C_1, C_2, C_3 and C_4.

tions to keep the trajectory on the desired orbit. Thus small, carefully chosen perturbations are able to effect a large beneficial change in the long-term system behaviour. If, on the other hand, the system dynamics were not chaotic but were, say, stable periodic, then small controls could only change the orbit slightly. We would then be closely restricted to whatever system performance the stable periodic orbit gave, and we would have no option for improvement using small controls.

Furthermore, one may want a system to be used for different purposes or under different conditions at different times. If the system is chaotic, this requirement might be accommodated without altering the gross configuration of the system. In particular, depending on the use desired, the system could be optimized by switching the temporal programming of the small controls to stabilize different orbits. By contrast, in the absence of chaos, completely separate systems might be required for each use. Thus, when designing a system, it may be advantageous to build chaos in, so as to achieve flexibility. For an experimental example, see Box 1. This experiment couples a magnetic field with a gravitationally buckling ribbon. Other recent relevant experiments have involved laser systems[10–14], electrical circuits[15], thermal convection[16] and arhythmically oscillating cardiac tissue (controlled using a small electrical stimulus)[18].

We will now consider examples of dynamical processes that we wish to control. A simple example might be a metre stick balanced on one's palm. This system is not chaotic and, provided that the stick does not stray too far from the vertical, it can be stabilized in its normally unstable, vertical state by making small motions of one's palm. This is an example of stabilizing an unstable steady state.

As a simple illustrative example of controlling a chaotic system we consider the 'Hénon map'[49]. Here the word 'map' refers to the fact that the time variable is discrete and integer-valued. The Hénon map is also described as a 'two-dimensional map'

BOX 1 Experimental confirmation

THE control of chaos by the application of tiny perturbations has been experimentally applied in several laboratories[14,17,29] (a modification, effective in stabilizing high-period orbits, appears in refs 10, 15). The first such application[9] used a nonlinear, inverted, magneto-elastic ribbon. This ribbon, sketched in Fig. B1, was clamped at its base but was otherwise free to move. The stiffness of the material was nonlinearly dependent on applied magnetic field, and in an oscillating field, applied by external field coils (not shown), the ribbon alternately buckled and stiffened in a complicated, chaotic pattern[76]. The position of the ribbon, $X(t)$, was measured at a point near its base using an optical sensor. By making small adjustments to the amplitude of the oscillating field (variations were less than 9% of its nominal value), the ribbon could be trapped in a variety of periodic motions. Figure B2 shows the ribbon displacement sampled once every oscillation of the applied magnetic field as a function of the number of periods, n. The sampling of the orbit at the drive period can be regarded as a "stroboscopic" surface of section. Initially no control was applied, leading to chaotic variation in the range of ribbon displacements between 2.7 and 4.4 on the vertical axis. Then, at about time $n \cong 2{,}200$, the control algorithm was activated to attempt to stabilize a period-1 orbit in the stroboscopic surface of section (compare this with Fig. 2*b*). After this orbit had been stabilized for over 2,000 oscillations, the control algorithm was switched at time $n \cong 4{,}900$ to try to stabilize a period-2 orbit (see Fig. 2*c*), and was later switched back to the period-1 orbit at $n \cong 7{,}100$.

The nonlinear ribbon was subsequently used to show that chaotic sensitivity can be used to actually direct trajectories in a chaotic system. By making small adjustments to the applied magnetic field (less than 5% of its nominal value), any trajectory could be quickly directed to a small target state. Figure B3 shows several successive trajectories which are rapidly brought from a variety of initial states, indicated by grey circles, to the target neighbourhood, $X = 2.5 \pm 0.01$. This target was chosen because it is ordinarily seldom visited: without control, the time to reach the chosen target was once in 500 iterations on average. By applying small perturbations, on the other hand, the target could typically be reached in less than once every 20 iterations.

We reiterate that the control was accomplished in real time and in the presence of experimental noise and modelling errors (to accommodate this, the targeting algorithm must be periodically reapplied; see refs 33, 35 for details). Additionally, the computational models used both for stabilization and for targeting were constructed entirely from available experimental data and without an *a priori* analytic model.

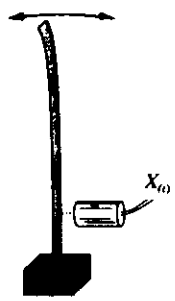

FIG. B1 Chaotic ribbon.

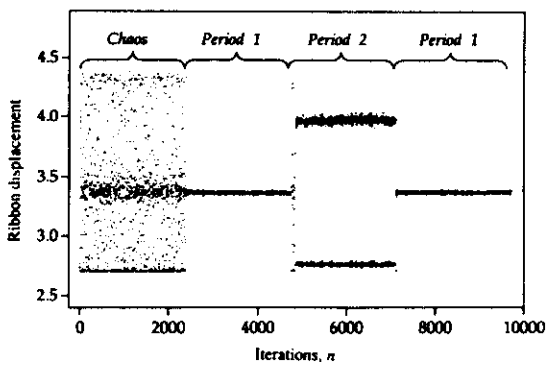

FIG. B2 Experimental stabilization of chaotic ribbon (reprinted with permission from ref. 9).

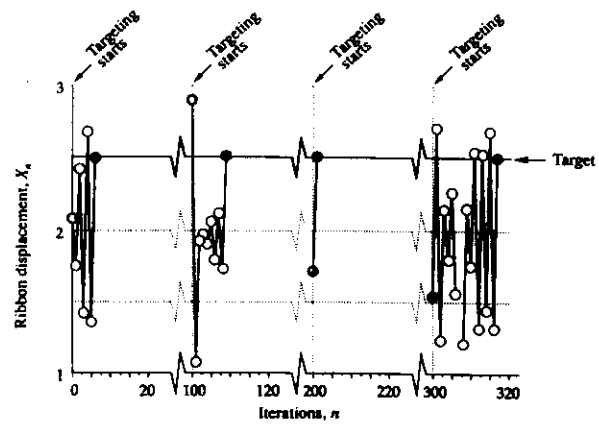

FIG. B3 Several successive realizations of targeting of a small neighbourhood of $X = 2.5$. Ribbon is allowed to wander chaotically between targeting attempts; targeting is initiated at $n = 0, 100, 200, 300$. With targeting, the neighbourhood of $X = 2.5$ is reached within 20 iterations; without targeting, the same neighbourhood is visited less than once every 500 iterations. The origin of the ordinate scale here differs from that of Fig. B2 because the optical sensor was moved between the times of the two experiments.

because the state of the system at time n (where $n = 0, 1, 2, \ldots$) is given by two scalar variables, x_n and y_n. The map specifies a rule for evolving the state of the system at time n to the state at time $(n+1)$. For the Hénon map, this rule is

$$x_{n+1} = p + 0.3y_n - x_n^2 \quad (1a)$$

$$y_{n+1} = x_n \quad (1b)$$

where the parameter p is set to a nominal value of $p_0 = 1.4$. Thus, given an initial state (x_1, y_1), the map allows us to calculate (x_2, y_2), which, when again inserted into the map, yields (x_3, y_3), and so on. Iterations of this map eventually converge to a strange attractor, as shown in Fig. 1. This structure is called an attractor because distant points are drawn toward it under successive iterations of the map, and it is called strange because it is infinitely intricate on every distance scale we might choose to examine. In the terminology of Mandelbrot, it is a fractal and has a fractal dimension of ~1.3. In the figure, we show just a few of the infinite number of embedded unstable periodic orbits; a period-1 point, A_*, which is revisited every map iteration, period-2 points, B_1 and B_2, each of which are revisited every other map iteration ($B_1 \to B_2 \to B_1 \to B_2 \ldots$), and period-4 points, $C_1 \ldots C_4$, which are cycled through every four map iterations.

Although the above example is a map (the time, n, is discrete), many problems in science and engineering involve continuous time, such as a system of M first-order, autonomous ordinary differential equations, $d\boldsymbol{\xi}/dt = \mathbf{G}(\boldsymbol{\xi})$, where $\boldsymbol{\xi}(t) = (\xi^{(1)}(t), \xi^{(2)}(t), \xi^{(3)}(t), \ldots, \xi^{(M)}(t))$ is an M-vector, and the continuous variable t denotes time. In such a case, discrete time systems are still of interest, as the M-dimensional continuous time system can be reduced to an $M-1$ dimensional map by the Poincaré surface-of-section technique illustrated in Fig. 2*a* for $M = 3$. Here we associate the continuous time trajectory with a discrete time trajectory, $\mathbf{Z}_1, \mathbf{Z}_2, \ldots$, where $\mathbf{Z}_n$ denotes an $M-1$ coordinate vector specifying the position on the surface of section of the nth upward piercing of the surface. Given a $\mathbf{Z}_n$, we can integrate the equation $d\boldsymbol{\xi}/dt = \mathbf{G}(\boldsymbol{\xi})$ forward in time from that point, until the next upward piercing of the surface of section, at the surface coordinates $\mathbf{Z}_{n+1}$. Thus $\mathbf{Z}_{n+1}$ is uniquely determined by $\mathbf{Z}_n$, and there must exist a map, $\mathbf{Z}_{n+1} = \mathbf{F}(\mathbf{Z}_n)$, from one trajectory point on the surface of section to the next. Although we may not be able to write down $\mathbf{F}$ explicitly, the knowledge that it exists is still useful. Figure 2*b* shows a periodic orbit of the continuous time system which results in a period-1 orbit of the associated Poincaré surface of section map: $\mathbf{Z}_* = \mathbf{F}(\mathbf{Z}_*)$. Figure 2*c* shows a periodic orbit of the continuous time system resulting in a period-2 orbit of the map: $\mathbf{Z}_2 = \mathbf{F}(\mathbf{Z}_1)$, $\mathbf{Z}_1 = \mathbf{F}(\mathbf{Z}_2)$.

Let us say that we have selected one of these unstable periodic orbits as providing the best performance of some hypothetical system. For simplicity, we consider the case where the desired orbit is a period-1 orbit of some N-dimensional map

$$\mathbf{Z}_{n+1} = \mathbf{F}(\mathbf{Z}_n, p) \quad (2)$$

where $\mathbf{Z}$ is an N-dimensional vector, and p denotes a system parameter. We first approximate the dynamics near the period-1 point, denoted $\mathbf{Z}_*$ (where $\mathbf{Z}_* = \mathbf{F}(\mathbf{Z}_*, p_0)$), for values of the parameter, p, close to the nominal value, p_0, by the linear map

$$(\mathbf{Z}_{n+1} - \mathbf{Z}_*) = \mathbf{A} \cdot (\mathbf{Z}_n - \mathbf{Z}_*) + \mathbf{B} \quad (p - p_0) \quad (3)$$

Here $\mathbf{A}$ is an $N \times N$ dimensional jacobian matrix and $\mathbf{B}$ is an N-dimensional column vector, where $\mathbf{A} = \partial\mathbf{F}/\partial\mathbf{Z}$, $\mathbf{B} = \partial\mathbf{F}/\partial p$, and these partial derivatives are evaluated at $\mathbf{Z} = \mathbf{Z}_*$ and $p = p_0$. We now assume that we can adjust the parameter p on each iteration. That is, we determine $\mathbf{Z}_n$ and on that basis make an appropriate small change in p from the nominal value p_0. Thus we replace p by p_n. Taking the control law to be linear, we have

$$(p_n - p_0) = -\mathbf{K}^T \cdot (\mathbf{Z}_n - \mathbf{Z}_*) \quad (4)$$

Here $\mathbf{K}$ is a constant N-dimensional column vector and $\mathbf{K}^T$ is its transpose. Choice of the vector $\mathbf{K}$ specifies the control law specifying p_n on each iteration. Substituting equation (4) into equation (3), we obtain

$$\delta\mathbf{Z}_{n+1} = (\mathbf{A} - \mathbf{B} \cdot \mathbf{K}^T)\delta\mathbf{Z}_n \quad (5)$$

where $\delta\mathbf{Z}_n = \mathbf{Z}_n - \mathbf{Z}_*$. Thus the period-1 point, $\mathbf{Z}_*$, will be stable if one can choose $\mathbf{K}$ so that the matrix $(\mathbf{A} - \mathbf{B} \cdot \mathbf{K}^T)$ only has eigenvalues with modulus smaller than unity. In this case, $\delta\mathbf{Z}_n \to 0$ (that is, $\mathbf{Z}_n \to \mathbf{Z}_*$) as $n \to \infty$. The choice of $\mathbf{K}$ represents a standard problem in control theory (for example, see ref. 50). (In fact, the matrix $(\mathbf{A} - \mathbf{B} \cdot \mathbf{K}^T)$ can be made to have any desired set of N eigenvalues provided that $\mathbf{B}$ satisfies a certain condition (called controllability[50]).) This procedure gives the time-dependent parameter values, p_n, required to stabilize an unstable period-1 point in a chaotic system. For the case of higher-period orbits, see ref. 4. We imagine that, because of practical constraints, we cannot make the deviations of p_n from p_0 too large. Thus we imagine that $|p_n - p_0|$ is bounded by some allowed maximum value, δp_{max}. Hence by equation (4), $\delta p_{max} > |\mathbf{K}^T \cdot (\mathbf{Z}_n - \mathbf{Z}_*)|$. If the system state is outside this region, we apply no perturbation and wait until the state falls within the

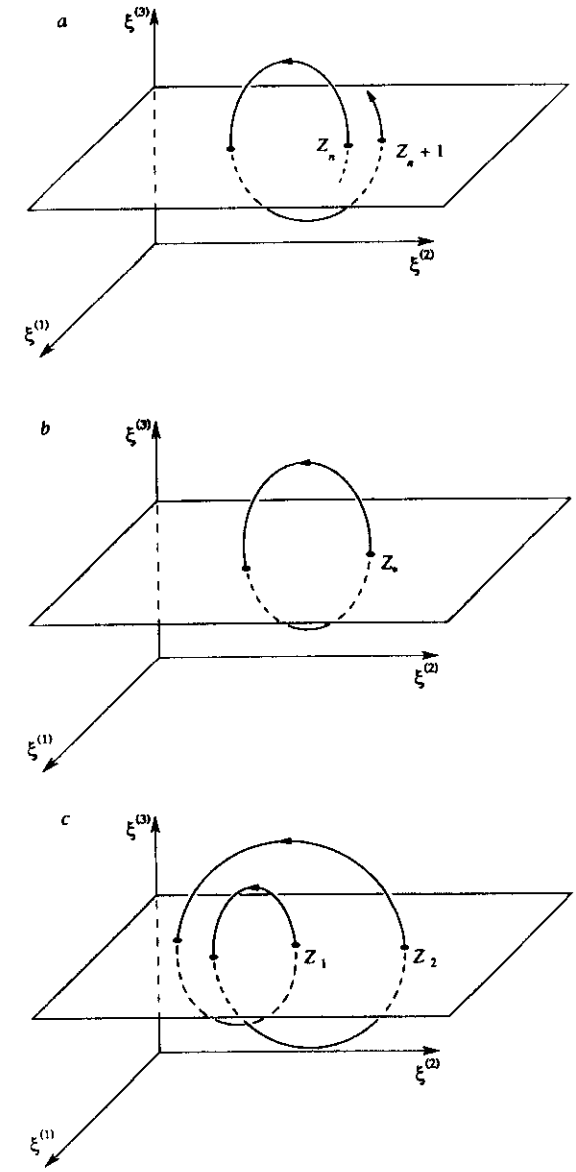

FIG. 2 *a*, The Poincaré surface-of-section technique. The surface of section, here shown for the case ξ_3 = constant, can, in principle, be chosen in any convenient way. *b*, Period-1 orbit; *c*, period-2 orbit.

given region. Once this occurs, we trap the system near the desired periodic state by applying the appropriate small nudges given by equation (4). Stabilization of the periodic points of the Hénon map by small perturbations is similar to stabilizing a vertical metre stick insofar as neither can be accomplished if the current state is far from the desired unstable state. We will discuss later how to direct a chaotic orbit to a neighbourhood of a desired state.

To illustrate stabilization of an unstable period-1 orbit in a more intuitive and geometrical manner, we consider the special case of a two-dimensional map where the desired period-1 orbit has one unstable and one stable direction. That is, there are two curves through $\mathbf{Z}_*$, called the stable manifold and the unstable manifold, as shown in Fig. 3*a*. We consider a small neighbourhood of $\mathbf{Z}_*$, so that the lines shown in Fig. 3 are roughly straight. An orbit starting from a point on the stable manifold remains on the stable manifold and moves exponentially toward $\mathbf{Z}_*$, whereas orbits of points on the unstable manifold move exponentially away from $\mathbf{Z}_*$. This corresponds to the case in which the matrix **A** has two real eigenvalues, one with magnitude less than one (stable), and one with magnitude greater than one (unstable). Also shown in Fig. 3*a* is a dashed line along which $\mathbf{Z}_*$ can be shifted by a change of the parameter p (this line is parallel to the vector **B**).

Imagine that the point $\mathbf{Z}_n$ falls close to $\mathbf{Z}_*(p_0)$, as shown in Fig. 3*a*. We now perturb the value of p from p_0 to $p_0+\delta p$, as shown in Fig. 3*b*. On the next iteration, the orbit is attracted towards $\mathbf{Z}_*(p_0+\delta p)$, in a direction parallel to its stable manifold, and, at the same time, is repelled from $\mathbf{Z}_*(p_0+\delta p)$ in a direction parallel to its unstable manifold. Thus if δp is chosen properly, we can cause $\mathbf{Z}_{n+1}$ to fall precisely on the stable manifold of $\mathbf{Z}_*(p_0)$. Thereafter, we can return the parameter to its nominal value, p_0, and the orbit will remain on the stable manifold of $\mathbf{Z}_*(p_0)$ and will approach $\mathbf{Z}_*(p_0)$. In terms of the more general discussion leading to equations (5), the above corresponds to a special choice of the control vector, **K**, such that one of the eigenvalues of $(\mathbf{A}-\mathbf{B}\cdot\mathbf{K}^T)$ is zero and the other is the original stable eigenvalue of **A**. As shown in ref. 4, this choice is optimal in that it minimizes the average time during which the orbit wanders chaotically before it can be stabilized.

As an example, in Fig. 4, we show the results of stabilizing the periodic orbit, $\mathbf{A}_*$, on the Hénon attractor by adjusting p by less than 1% of its nominal value. Starting at a random initial point on the attractor, we see that for the first 86 iterations, the trajectory moves chaotically on the attractor, never falling within the desired small region about $\mathbf{A}_*$. Then, on the 87th iteration, the state falls within the desired region, and thereafter is held near $\mathbf{A}_*$. In the presence of noise, the stabilization procedure would have to be regularly reapplied (see ref. 3 for details).

The control strategy need not rely on an *a priori* analytical model. Just as one can balance a metre stick on the palm without knowing anything at all about Newton's equations of motion for the stick, one can produce effective stabilization for more complicated systems without an explicit set of differential equations. By empirical study of the effects of small parameter changes on orbits near a desired periodic state, an arbitrary periodic state in a chaotic attractor can be stabilized using only small controls (see Box 1). This is important because in experimental situations one may often not have on hand an accurate analytical model.

Figure 5 illustrates how knowledge of a periodic orbit, the matrix **A**, and the vector **B** can all be extracted purely from observations of the trajectory on the strange attractor. Imagine that we collect a long data string of observed surface-of-section piercings, $\mathbf{Z}_1, \mathbf{Z}_2$ and so on. If two successive **Z**s are close to each other, say $\mathbf{Z}_{100}$ and $\mathbf{Z}_{101}$, then there will typically be a period-1 orbit $\mathbf{Z}_*$ nearby[47,48] (Fig. 5). Having observed a first such close return, we then search the succeeding data for other close-return pairs $(\mathbf{Z}_n, \mathbf{Z}_{n+1})$ restricted to the small region of the original close return (shown shaded in Fig. 5). Because orbits on a strange attractor are ergodic, we will have many such pairs if the data string is long enough. Assuming the shaded region to be small, we then try to fit these close returning pairs with a linear relation

$$\mathbf{Z}_{n+1}=\hat{\mathbf{A}}\cdot\mathbf{Z}_n+\hat{\mathbf{C}} \qquad (6)$$

Generally, if there is noise in the data, we would want to use as many pairs as possible and fit the matrix $\hat{\mathbf{A}}$ and the vector $\hat{\mathbf{C}}$ using a least-squares fit to the data. Thus $\hat{\mathbf{A}}$, the least-squares fit matrix, is an approximation to the jacobian matrix **A** of equation (3), and the period-1 point, $\mathbf{Z}_*(p)$, is approximated by $(1-\hat{\mathbf{A}})^{-1}\cdot\hat{\mathbf{C}}$. To find **B** of equation (3), we change p slightly, $p\to p+\Delta p$, redetermine the period-1 point $\mathbf{Z}_*(p+\Delta p)$ as before, and approximate **B** as $[\mathbf{Z}_*(p+\Delta p)-\mathbf{Z}_*(p)]/\Delta p$. To find period-2 orbits, we proceed in the same way, but for pairs $(\mathbf{Z}_n, \mathbf{Z}_{n+2})$ that are close after two surface-of-section piercings (and similarly for higher periods).

In experimental studies of chaotic dynamics, it is often helpful to use 'delay coordinate embedding'[51,52]. These allow one to obtain information on the topological phase space structure of an attractor even when one cannot directly measure the instantaneous system state vector, ξ, which we take to be M-dimensional. As a typical example, the time history of only a single scalar variable, say $\phi(t)$, might be the only thing that one

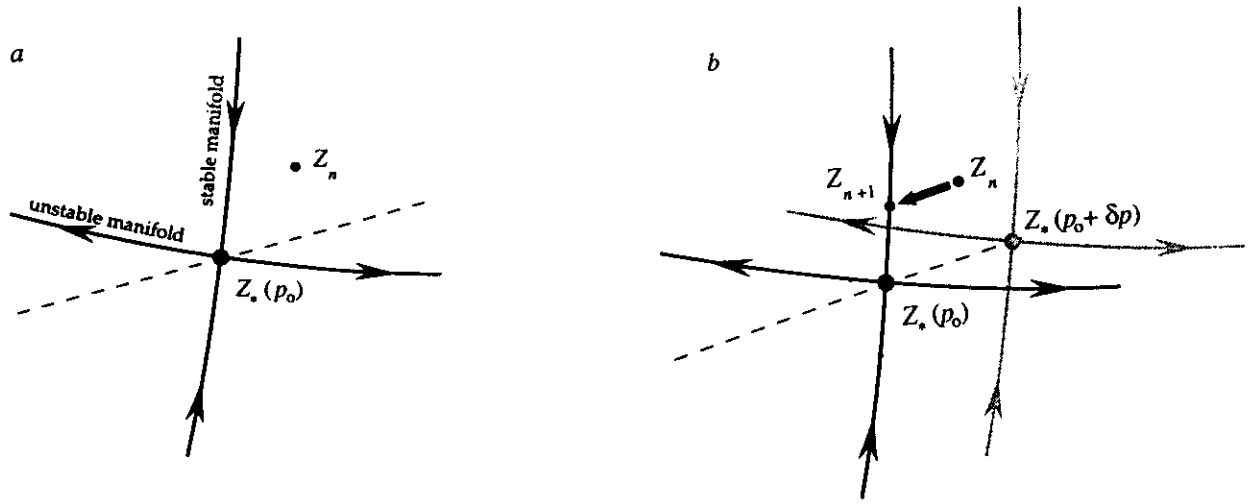

FIG. 3 *a*, The period-1 point, $\mathbf{Z}_*(p_0)$, its stable and unstable manifolds (solid lines), and the line (dashed) along which $\mathbf{Z}_*$ can be shifted by perturbation of the parameter p. *b*, Result of perturbing p to $p_0+\delta p$; the stable and unstable manifolds of $\mathbf{Z}_*(p_0+\delta p)$ are shown as grey lines through $\mathbf{Z}_*(p_0+\delta p)$.

can measure experimentally. To proceed, one forms the Q-dimensional 'delay coordinate vector'

$$\Phi(t) = (\phi(t), \phi(t-T_D), \phi(t-2T_D), \ldots, \phi(t-(Q-1)T_D)) \quad (7)$$

where T_D is some conveniently chosen delay time. Embedding theorems[53,54] guarantee that for $Q \geq 2M+1$, the vector $\Phi(t)$ is generically a global one-to-one representation of the system state. (Actually, for our purposes we do not require a global embedding; we only require a one-to-one correspondence in the small region near the periodic orbit, and this can typically be achieved with $Q = M$.) To obtain a discrete time series from $\Phi(t)$, we can again use a Poincaré surface of section, but this time in Φ-space. Let $\tilde{\mathbf{Z}}_n$ denote points in the Φ-space surface of section, and let the corresponding surface-of-section map for a constant value of the parameter p be denoted $\tilde{\mathbf{Z}}_{n+1} = \tilde{F}(\tilde{\mathbf{Z}}_n, p)$. As pointed out in ref. 7, in the presence of parameter variation ($p \to p_n$), delay coordinates lead to a map of a form other than $\tilde{\mathbf{Z}}_{n+1} = \tilde{F}(\tilde{\mathbf{Z}}_n, p_n)$, which is the form assumed for equations (3) and (4). As an example, say that the time interval T_n between the surface-of-section piercing at $\tilde{\mathbf{Z}}_n$ and at $\tilde{\mathbf{Z}}_{n+1}$ is such that

$$rT_n \geq (Q+1)T_D > (r-1)T_n \quad (8)$$

where r is an integer. Then the relevant map is of the form

$$\tilde{\mathbf{Z}}_{n+1} = \tilde{F}(\tilde{\mathbf{Z}}_n, p_n, p_{n-1}, \ldots, p_{n-r}). \quad (9)$$

This follows because $\Phi(t_n)$, where t_n denotes the nth piercing of the surface of section (corresponding to $\tilde{\mathbf{Z}}_n$), has components $\phi(t_n), \ldots, \phi(t_n-(Q-1)T_D)$ and hence $\tilde{\mathbf{Z}}_n$ must depend, not only on p_n, but also on all the other parameter values in effect during the time interval $t_n \leq t \leq [t_n-(Q-1)T_D]$. For discussion of how the analysis of equations (3) to (5) can be extended to the case of delay coordinates, see refs 4 and 7.

Although the approach just described provides a systematic means of choosing a feedback algorithm, it will often be the case (particularly when the dynamics are low-dimensional) that a trial and error procedure will succeed[10,15]: simply choose some feedback law (arbitrarily choose $\mathbf{K}$ in equation (4)) and vary it until it is observed that the desired orbit stabilizes. (Knowledge of the periodic orbit location in phase space is still required, so a procedure such as that of Fig. 5 may still be necessary.)

Further discussion of stabilization

We now briefly discuss some other considerations relevant to the stabilization of unstable periodic orbits and steady states embedded in strange attractors. One issue is related to bifurcations. The word bifurcation, when applied to a periodic orbit or steady state, refers to a change in the character of the orbit from stable to unstable while the system is continuously changed. Often the nset of chaos comes about as a result of bifurcations of periodic orbits or steady states. Two well known cases are the commonly observed cascade of period-doubling bifurcations preceding chaos, and the onset of chaos when a steady state bifurcates from stable to unstable. Thus one way of controlling chaos is to prevent or change the character of these bifurcations. This has been discussed in refs 18 and 19, where control methods that are insensitive to errors in the knowledge of the system are used. In this regard, we also mention the laser experiments of refs 12 and 13.

Control can also be used as a means of tracking the location of unstable orbits as the system is changed[21,22]. In a recent experiment, this technique was used to increase the stable steady power output of a laser by an order of magnitude[17]. Another issue is that of prescribing controls that are assured of bringing the trajectory to the desired periodic orbit or steady state. This has been addressed using the Lyapunov function method[16,23].

Other interesting work in this general area includes the use of the describing function technique of control theory for finding and controlling unstable periodic orbits[24]; control of unstable chaotic sets (as opposed to chaotic attractors)[25]; the control of homoclinic orbits[26]; and control of aperiodic orbits[55].

Directing chaotic trajectories

Stabilizing a system by small perturbations is extremely effective once the system at hand comes close to the desired state. But if it starts far from the desired state, it might take an unacceptably long time before a typical orbit comes close enough to the desired state to be captured. We now discuss how small perturbations, applied when the orbit is far from the desired state, can be used to steer the system to this state. For example, chaotic rhythms in cardiac tissue can be stabilized as outlined above[17]. What if one wants to stabilize a regular rhythm in the heart without having the luxury of simply waiting for the system to fall near a desired state? It is, moreover, intrinsically desirable to be able to steer a system to a general target in phase space (not necessarily a periodic orbit). NASA's mission specialists demonstrated this when, as mentioned earlier, they achieved the first scientific cometary encounter by steering the spacecraft ISEE-3/ICE in a complex trajectory using only small nudges from the spacecraft's dwindling fuel supply[39-43].

The application of chaotic sensitivity to steer trajectories to targets in chaotic systems using small controls is discussed in refs 33-37; related work appears in refs 38 and 55. To understand the idea in its simplest form, consider the well known logistic map (see for example ref. 56):

$$X_{n+1} = pX_n(1-X_n) \quad (10)$$

where we take a nominal value of 3.9 for p. This map is used to describe the behaviour of a population of organisms after successive years, where n denotes the year. In this case, X represents the (normalized) population, and p defines its growth rate per year when the population is small. For any X between 0 and 1, it is easy, using only a pocket calculator, to adjust the growth rate slightly so that any given target, again between 0 and 1, is quickly reached.

Suppose for example that the current state is $X_1 = 0.4$ and we want to reach the vicinity of $X_n = 0.8$. If we can adjust p during the first year by a small amount, say between 3.8 and 4.0, then after one year, the population can range between $X_2 = 0.91$ and $X_2 = 0.96$. We then return to the nominal parameter value, $p = 3.9$, and after a second year the range grows to cover from $X_3 = 0.15$ to $X_3 = 0.31$. After a third year, the range grows even more to extend from $X_4 = 0.50$ to $X_4 = 0.84$. As our target, $X = 0.8$, is in this range, there must be some value of p_1 in the

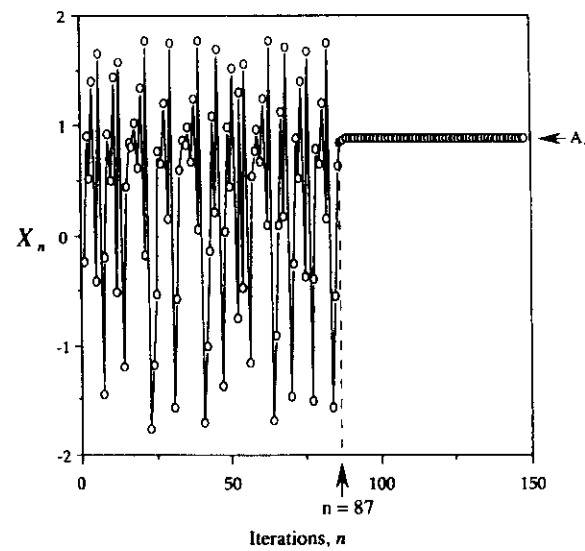

FIG. 4 Stabilization of the period-1 state for the Hénon map.

range $3.8 \leq p_1 \leq 4.0$ such that when p is shifted to that value in the first year, X falls on the target in only three years. Indeed, a little work with our pocket calculator reveals that we can reach our target by setting $p_1 = 3.83189...$. We emphasize that it is possible to accomplish this only because the logistic system is chaotic, and because chaotic systems are characterized by the exponential growth of small disturbances. This exponential growth implies that we can reach any accessible target extremely quickly (that is, in a time of the order of the logarithm of the maximum allowed size of the small parameter perturbation), using only a small perturbation.

As another example, consider the equations

$$\frac{dX}{dt} = \sigma(Y - X) \tag{11a}$$

$$\frac{dY}{dt} = -XY - Y + r + p(t) \tag{11b}$$

$$\frac{dZ}{dt} = XY - bZ \tag{11c}$$

which (for $p(t) \equiv 0$) were introduced[57] by Lorenz as a simplified model of chaotic fluid thermal convection. The Lorenz equations provide a leading-order description of the dynamics of a fluid contained in a thin vertically oriented torus with a heat source applied at the bottom[58]. The equations with $p(t) \equiv 0$ have a strange attractor for the parameter values $\sigma = 10$, $r = 28$, $b = 8/3$, and an orbit on this chaotic attractor is shown in blue in Fig. 6. The steady state, $X(t) = Y(t) = Z(t) = 0$, representing no fluid convection, is a solution of the Lorenz equations. Furthermore, this solution is contained in the chaotic attractor. Note from Fig. 6 that the blue finite-duration orbit does not reach anywhere near this steady state (the open circle in the figure). If the orbit were followed long enough, it would eventually come arbitrarily near the stationary state. We estimate that of the order of one in 10^{10} orbits around either of the lobes of the attractor ever passes through a sphere of radius 0.1 centred at $X = Y = Z = 0$. (For comparison, the blue trajectory in Fig. 6 shows only about 20 orbits around either lobe of the attractor.) For the purpose of demonstrating control of the Lorenz system we have added the term $p(t)$ to the right-hand side of equation (11b). For the physical situation of a vertically oriented fluid-filled torus, the term $p(t)$ represents a perturbation of the position of the heat source slightly to the left or right in the plane of the torus ($p = 0$ corresponds to heating exactly at the bottom of the torus). Restricting the perturbations, $p(t)$, to be small, $|p(t)| < 0.01$, it typically takes of the order of 10 orbits around a lobe to reach the origin (as compared, again, with 10^{10} orbits to reach $\sqrt{X^2 + Y^2 + Z^2} < 0.1$ when no control is applied). Figure 6 shows such an orbit in red. The method for programming the perturbations is described in ref. 36 and is similar in principle to that which we have described for the logistic map, equation (10).

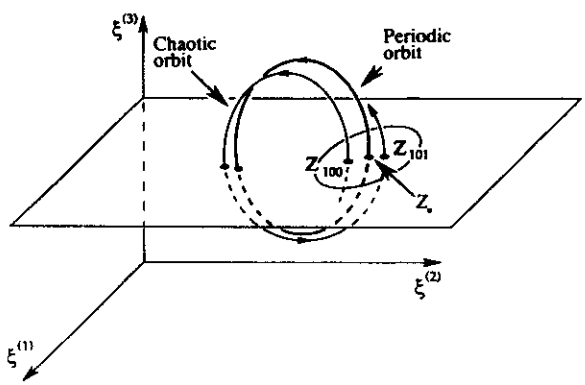

FIG. 5 Determining unstable periodic point, $\mathbf{Z}$ from data, $\mathbf{Z}_{100}$, $\mathbf{Z}_{101}$ ....

The preceding example illustrates the idea of targeting. More detailed descriptions and methods can be found in refs 33–38. One technique is to patch together different trajectories to reach a desired target state. These trajectories can originate in a single chaotic system with differing parameter values[37,38], or from a systematic examination of small changes in the system state[39–43]. NASA's manoeuvre of the spacecraft ISEE-3/ICE is such a case. Five separate swings past the Moon were combined to produce the final spacecraft trajectory. By inventive choices of intermediate trajectories, researchers have shown this technique to be effective in matching greatly differing initial and final state vectors.

At this point, we must make two remarks. First, the sensitivity of chaotic systems allows us to produce large changes in the orbit of the system after some time using tiny perturbations, but the same sensitivity makes the final state depend on ubiquitous noise. The noise, if small enough, can be compensated for, however, by periodically reapplying the targeting algorithm, thereby obtaining mid-course corrections of the parameter perturbation (see Box 1 and refs 33 and 35). Second, one needs a global model of the system in order to direct trajectories. This differs from the stabilization of periodic orbits or steady states, where one only needs local information, near the desired periodic orbit. In general, this makes the use of experimental delay coordinate techniques for application to targeting more difficult. Nevertheless, in some cases it may be possible (Box 1).

The control of chaos by small perturbations has been developed into a proposed application for communication[59]. Consider the 'double scroll' electrical oscillator[60], which yields a chaotic signal consisting of a seemingly random sequence of positive and negative peaks. If we associate a positive peak with a one and a negative peak with a zero, the signal yields a binary sequence. With small control perturbations, we can cause the signal to follow an orbit whose binary sequence represents the information we wish to communicate. (Here our 'target' is a particular binary sequence rather than a point in phase space.) Hence the chaotic power stage that generates the waveform for transmission can remain simple and efficient (complex chaotic behaviour occurs in simple systems), while all the complex electronics controlling the output can remain at the low-power microelectronic level.

Other ways to alter chaotic dynamics

We have focused here on work using the sensitivity of chaotic systems to stabilize existing chosen periodic orbits and steady states and to steer trajectories with only small controls. Several authors have developed other techniques to alter the dynamics of chaotic systems without explicitly using this sensitivity, and in this section, we summarize some of their key contributions.

One body of research[61–68] seeks to control a nonlinear system to follow a prescribed goal dynamics. If we denote the system by

$$\frac{d\boldsymbol{\xi}}{dt} = \mathbf{F}(\boldsymbol{\xi}) + \mathbf{U}(t) \tag{12}$$

where $\mathbf{U}(t)$ is an additive controlling term, then the object is to choose $\mathbf{U}(t)$ so that $|\boldsymbol{\xi}(t) - \mathbf{g}(t)| \to 0$ as $t \to \infty$, where $\mathbf{g}(t)$ is the goal dynamics. To accomplish this, the simple choice

$$\mathbf{U}(t) = \frac{d\mathbf{g}}{dt} - \mathbf{F}(\mathbf{g}(t)) \tag{13}$$

is made. Thus $\boldsymbol{\xi}(t) = \mathbf{g}(t)$ is clearly a solution of the controlled equations. What is not so clear is that convergence to this goal will often occur ($|\boldsymbol{\xi}(t) - \mathbf{g}(t)| \to 0$ as $t \to \infty$). Whether it does so depends on the particular $\mathbf{F}$ and the initial condition, $\boldsymbol{\xi}(0)$. The regions of $\boldsymbol{\xi}$-space such that controlled orbits originating in them converge to the goal, $\mathbf{g}$, are called entrainment regions[64–66]. This method potentially works for nonlinear systems in general (not necessarily chaotic) and has the advantage of not requiring

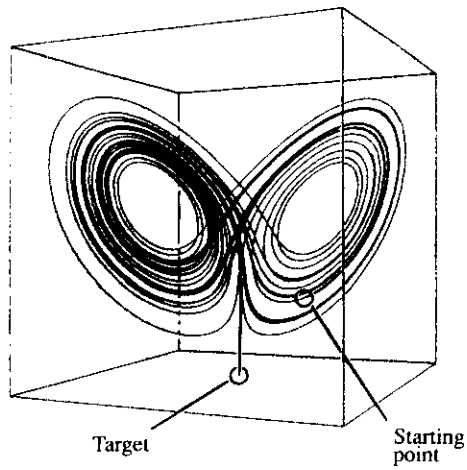

FIG. 6 Targeting of steady state in Lorenz attractor. Blue; trajectory without control; red: trajectory with control.

feedback. On the other hand, the applied controls are not typically small and convergence to the goal is not assured.

Another body of research addresses the effects of periodic[69-73] and stochastic[74,75] perturbations on chaotic systems. As one might expect, the effects of such perturbations can be quite difficult to predict in general, and indeed these studies are not 'goal oriented', in that a desired behaviour is not specified in advance and a generic technique for achieving such a goal has not been developed. Nevertheless, dramatic changes in the dynamics of chaotic systems have been recorded using these methods; for example, periodic or nearly periodic behaviour can sometimes be produced from originally chaotic dynamical systems.

The advantages of chaos

The presence of chaos may be a great advantage for control in a variety of situations. In a nonchaotic system, small controls typically can only change the system dynamics slightly. Short of applying large controls or greatly modifying the system, we are stuck with whatever system performance already exists. In a chaotic system, on the other hand, we are free to choose between a rich variety of dynamical behaviours. Thus we anticipate that it may be advantageous to design chaos into systems, allowing such variety without requiring large controls or the design of separate systems for each desired behaviour.

The general problem of controlling chaotic systems is very rich, and may help solve technologically important problems in widely diverse fields of study. In communications, it has been proposed that chaotic fluctuations can be put to use to send controlled, pre-planned signals[59]. In physiology, applications have been proposed for controlling chaos in the heart[17] and in neural information processing[27]. In fluid mechanics, it has been demonstrated in a simple configuration that chaotic convection[16] can be controlled. Chemical researchers have developed mechanisms for controlling chaotic autocatalytic reactions[28]. Chaotic lasers[10,11] have been controlled, as has the chaotic diode circuit[15]. The wealth of results such as these encourage us to look forward to a fruitful future for the control of chaotic systems. □

Troy Shinbrot is at the Department of Physics and Institute for Physical Science and Technology, University of Maryland, College Park, Maryland 20742, USA; present address for Troy Shinbrot is Laboratory for Fluid Mechanics, Chaos and Mixing, Northwestern University, Evanston, Illinois 60208, USA. Celso Grebogi and James A. Yorke are at the Department of Mathematics and Institute for Physical Science and Technology, University of Maryland, College Park, Maryland 20742, USA. Edward Ott is at the Department of Electrical Engineering, the Department of Physics and the Institute for Systems Research, University of Maryland, College Park, Maryland 20742, USA.

1. Dyson, F. *Infinite in All Directions*, 183–184 (Harper and Row, New York, 1988).
2. Ott, E., Grebogi, C. & Yorke J. A. *Phys. Rev. Lett.* **64**, 1196–1199 (1990).
3. Ott, E., Grebogi, C. & Yorke, J. A. in *Chaos: Soviet–American Perspectives on Nonlinear Science* (ed. Campbell, D. K.) 153–172 (Am. Inst. Phys., New York, 1990).
4. Ott, E., Romeiras, F. J., Grebogi, C. & Dayawansa, W. P. *Physica* D **58**, 165–192 (1992).
5. Auerbach, D., Grebogi, C., Ott, E. & Yorke, J. A. *Phys. Rev. Lett.* **69**, 3479–3482 (1992).
6. Fowler, T. B. *IEEE Trans. Auto. Control* **34**, 201–205 (1989).
7. Dressler, U. & Nitsche, G. *Phys. Rev. Lett.* **68**, 1–4 (1992).
8. Pyragas, K. *Phys. Lett.* **A170**, 421–428 (1992).
9. Ditto, W. L., Rauseo, S. N. & Spano, M. L. *Phys. Rev. Lett.* **65**, 3211–3214 (1990).
10. Roy, R., Murphy, T. W., Maier, T. D., Gills, A. & Hunt, E. R. *Phys. Rev. Lett.* **68**, 1259–1262 (1992).
11. Gills, Z., Iwata, C., Roy, R., Schwartz, I. B. & Triandaf, I. *Phys. Rev. Lett.* **69**, 3169–3172 (1992).
12. Bielawski, S., Bouazaoui, M., Derozier, D. & Glorieux, P. *Proc. Nonlinear Dynam. Optical Syst. Topical Mtg, Alpbach, Austria, June 22–26* (Optical Society of America, Washington, DC 1992).
13. Bielawski, S., Bouazaoui, M., Derozier, D. & Glorieux, P. *Stabilization and Characterization of Unstable Steady States in a Laser* (preprint, 1992).
14. Reyt, C., Flepp, L., Badii, R. & Brun, E. *Control of NMR-laser Chaos in High-dimensional Embedding Space* (preprint, 1992).
15. Hunt, E. R. *Phys. Rev. Lett.* **67**, 1953–1955 (1991).
16. Singer, J., Wang, Y. Z. & Bau, H. H. *Phys. Rev. Lett.* **66**, 1123–1125 (1991).
17. Garfinkel, A., Spano, M. L., Ditto, W. L. & Weiss, J. N. *Science* **257**, 1230–1235 (1992).
18. Abed, E. H., Wang, H. O. & Lee, H.-C. *Proc. 1992 Am. Control Conf.*, 2236–2237 (Chicago, 1992).
19. Wang, H. O. & Abed, E. H. *Proc. 2nd IFAC Workshop Syst. Struct. Control*, 494–497 (Prague, 1992).
20. Wang, H. O. & Abed, E. H. *Proc. 2nd IFAC Nonlinear Control Sys. Design Symp.*, 57–62 (Bordeaux, France, June 1992).
21. Schwartz, I. B. & Triandaf, I. *Phys. Rev.* **A46**, 7439–7444 (1992).
22. Carroll, T., Triandaf, I., Schwartz, I. B. & Pecora, L. *Phys. Rev.* **A46**, 6189–6192 (1992).
23. Chen, G. & Dong, X. *J. Circ. Syst. Comput.* **3** (in the press).
24. Genesio, R. & Tesi, A. *Automatica* **28**, 531–548 (1992).
25. Tél, T. *J. Phys.* **A24**, L1359–L1368 (1992).
26. Bloch, A. M. & Marsden, J. E. *Theor. comput. Fluid Dynam.* **1**, 179–190 (1989).
27. Ding, M. & Kelso, J. A. S. in *Measuring Chaos in the Human Brain* (eds Duke, D. & Pritchard, W.) 17–31 (World Scientific, Singapore, 1991).
28. Petrov, V., Gáspár, V., Masere, J. & Showalter, K. *Nature* **361**, 240–243 (1993).
29. Hübinger, B., Doerner, R. & Martienssen, W. *Controlling Chaotic Motion in Noisy Systems* (preprint, Phys. Inst. der J. W. Goethe-Universität, Frankfurt-am-Main, 1992).
30. Vassiliadis, D. *Physica* D (in the press).
31. Huberman, B. A. & Lumer, E. *IEEE Trans. Circ. Syst.* **37**, 547–550 (1990).
32. Sinha, S. & Ramaswamy, R. *Physica* **D43**, 118–128 (1990).
33. Shinbrot, T., Ott, E., Grebogi, C. & Yorke, J. A. *Phys. Rev. Lett.* **65**, 3215–3218 (1990).
34. Shinbrot, T., Ott, E., Grebogi, C. & Torke, J. A. *Phys. Rev.* **A45**, 4165–4168 (1992).
35. Shinbrot, T., Ott, E., Grebogi, C. & Yorke, J. A. *Phys. Rev. Lett.* **68**, 2863–2866 (1992).
36. Shinbrot, T., Grebogi, C., Ott, E. & Yorke, J. A. *Phys. Lett.* **A169**, 349–354 (1992).
37. Kostelich, E., Grebogi, C., Ott, E. & Yorke, J. A. *Phys. Rev.* **E47**, 305–310 (1993).
38. Bradley, E. in *Lecture Notes Control and Information Sciences*, No. 165 (eds Jacob, G. & Lamnabhi-Lagarrigue, F.) 307–325 (Springer, Berlin, 1991).
39. Farquhar, R., Muhonen, D. & Church, L. C. *J. astronaut. Sci.* **33**, 235–254 (1985).
40. Muhonen, D., Davis, S. & Dunham, D. *J. astronaut. Sci.* **33**, 255–273 (1985).
41. Dunham, D. W. & Davis, S. A. *J. astronaut. Sci.* **33**, 275–288 (1985).
42. Muhonen, D. & Folta, D. *J. astronaut. Sci.* **33**, 289–300 (1985).
43. Efron, L., Yeomans, D. K. & Schanzle, A. F. *J. astronaut. Sci.* **33**, 301–323 (1985).
44. So, P., Ott, E. & Dayawansa, W. P. *Phys. Lett.* A. (in the press).
45. Chen, G. & Dong, X. *From Chaos to Order—Perspectives and Methodologies in Controlling Chaotic Dynamical Systems Tech. Rep. 92-07* (Univ. Houston, Texas, 1992).
46. Vincent, T. L. & Yu, *J. Dynam. Control* **1**, 35–52 (1991).
47. Grebogi, C., Ott, E. & Yorke, J. A. *Phys. Rev.* **A37**, 1711 (1988).
48. Auerbach, D., Cvitanović, P., Eckmann, J.-P., Gunaratne, G. & Procaccia, I. *Phys. Rev. Lett.* **58**, 2387 (1987).
49. Hénon, M. *Commun. Math. Phys.* **50**, 69–77 (1976).
50. Ogata, K. *Modern Control Engineering*, 2nd Ed. 347–889 (Prentice-Hall, Englewood Cliffs, 1990).
51. Packard, N. H., Crutchfield, J. P., Farmer, J. D. & Shaw, R. S. *Phys. Rev. Lett.* **45**, 712–716 (1980).
52. Eckmann, J.-P. & Ruelle, D. *Rev. mod. Phys.* **57**, 617–656 (1985).
53. Whitney, H. *Ann. Math.* **37**, 645–671 (1936).
54. Takens, F. in *Lecture Notes in Mathematics 898* (eds Rand, D. A. & Young, L. S.) 366–381 (Springer, Berlin, 1981).
55. Mehta, N. J. & Henderson, R. M. *Phys. Rev.* **A44**, 4861–4865 (1991).
56. Schuster, H. G. *Deterministic Chaos*, 2nd ed., 37–38 (VCH, Weinheim, 1989).
57. Lorenz, E. *J. atmos. Sci.* **20**, 130–141 (1963).
58. Yorke, J. A., Yorke, E. D. & Mallet-Paret, J. *Physica* **D24**, 279–291 (1987).
59. Hayes, S., Grebogi, C. & Ott, E. *Phys. Rev. Lett.* **70**, 3031–3034 (1993).
60. Chua, L. O., Komura, M. & Matsumoto, T. *IEEE Trans. Circ. Syst.* **11**, 1073–1118 (1986).
61. Hübler, A. & Lüscher, E. *Naturwissenschaften* **76**, 67–69 (1989).
62. Hübler, A. W. *Helv. phys. Acta* **62**, 343–346 (1989).
63. Plapp, B. B. & Hübler, A. W. *Phys. Rev. Lett.* **65**, 2302–2305 (1990).
64. Jackson, E. A. & Hübler, A. W. *Physica* **D44**, 407–420 (1990).
65. Jackson, E. A. *Phys. Lett.* **A151**, 478–484 (1990).
66. Jackson, E. A. *Phys. Rev.* **A44**, 4839–4853 (1991).
67. Lüscher, E. & Hübler, A. W. *Helv. phys. Acta* **62**, 544–551 (1989).
68. Georgii, R., Eberl, W. & Lüscher, E. *Helv. phys. Acta* **62**, 290–293 (1989).
69. Alekseev, V. V. & Loskutov, A. Y. *Sov. Phys. Dokl.* **32**, 1346–1348 (1987).
70. Pettini, M. in *Dynamics and Stochastic Processes* (ed. Lima, R., Streit, L. & Vilela Mendes, R. 242–250 (Springer, Berlin, 1990).
71. Lima, R. & Pettini, M. *Phys. Rev.* **A41**, 726–733 (1990).
72. Braiman, Y. & Goldhirsch, I. *Phys. Rev. Lett.* **66**, 2545–2548 (1991).
73. Azevedo, A. & Rezende, S. M. *Phys. Rev. Lett.* **66**, 1342–1345 (1991).
74. Herzel, H. *A. Angew. Math. Mech.* **68**, 11–12 (1988).
75. Fahy, S. & Hamann, D. R. *Phys. Rev. Lett.* **69**, 761–764 (1992).
76. Ditto, W. L. *et al. Phys. Rev. Lett.* **63**, 923–966 (1989).
77. Lai, Y.-C., Ding, M.-Z. & Grebogi, C. *Phys. Rev.* **E47**, 86–92 (1992).
78. Abed, E. H., Wang, H. O. & Chen, R. *Physica* D (in the press).

ACKNOWLEDGEMENTS. This work was supported by the United States Department of Energy (Office of Scientific Computing, Office of Energy Research). We thank D. Auerbach, G. R. Chen, A. Hübler and K. Scarbrough for helpful comments. W. Ditto, S. Rauseo and M. Spano are gratefully acknowledged for providing data for this article.

Controlling Chaos

Edward Ott,[a],[b] Celso Grebogi,[a] and James A. Yorke[c]
University of Maryland, College Park, Maryland 20742
(Received 22 December 1989)

It is shown that one can convert a chaotic attractor to any one of a large number of possible attracting time-periodic motions by making only *small* time-dependent perturbations of an available system parameter. The method utilizes delay coordinate embedding, and so is applicable to experimental situations in which *a priori* analytical knowledge of the system dynamics is not available. Important issues include the length of the chaotic transient preceding the periodic motion, and the effect of noise. These are illustrated with a numerical example.

PACS numbers: 05.45.+b

The presence of chaos in physical systems has been extensively demonstrated and is very common. In practice, however, it is often desired that chaos be avoided and/or that the system performance be improved or changed in some way. Given a chaotic attractor, one approach might be to make some large and possibly costly alteration in the system which completely changes its dynamics in such a way as to achieve the desired behavior. Here we assume that this avenue is not available. Thus, we address the following question: Given a chaotic attractor, how can one obtain improved performance and a desired attracting time-periodic motion by making only *small* time-dependent perturbations in an *accessible* system parameter?

The key observation is that a chaotic attractor typically has embedded within it an infinite number of unstable periodic orbits.[1] Since we wish to make only small perturbations to the system, we do not envision creating new orbits with very different properties from the existing ones. Thus, we seek to exploit the already existing unstable periodic orbits. Our approach is as follows: We first determine some of the unstable low-period periodic orbits that are embedded in the chaotic attractor. We then examine these orbits and choose one which yields improved system performance. Finally, we tailor our small time-dependent parameter perturbations so as to stabilize this already existing orbit. In this Letter we describe how this can be done, and we illustrate the method with a numerical example. The method is very general and should be capable of yielding greatly improved performance in a wide variety of situations.

It is interesting to note that if the situation is such that the suggested method is practical, then the presence of chaos can be a great advantage. The point is that any one of a number of different orbits can be stabilized, and the choice can be made to achieve the best system performance among those orbits. If, on the other hand, the attractor is not chaotic but is, say, periodic, then small parameter perturbations can only change the orbit slightly. Basically we are then stuck with whatever system performance the stable periodic orbit gives, and we have no option for substantial improvement, short of making large alterations in the system.

Furthermore, one may want a system to be used for different purposes or under different conditions at different times. Thus, depending on the use, different requirements are made of the system. If the system is chaotic, this type of multiple-use situation might be accommodated without alteration of the gross system configuration. In particular, depending on the use desired, the system behavior could be changed by switching the temporal programming of the small parameter perturbations to stabilize different orbits. In contrast, in the absence of chaos, completely separate systems might be required for each use. Thus, when designing a system intended for multiple uses, purposely building chaotic dynamics into the system may allow for the desired flexibility. Such multipurpose flexibility is essential to higher life forms, and we, therefore, speculate that chaos may be a necessary ingredient in their regulation by the brain.

To simplify the analysis we consider continuous-time dynamical systems which are *three dimensional* and depend on one system parameter which we denote p [for example, $d\mathbf{x}/dt=\mathbf{F}(\mathbf{x},p)$, where $\mathbf{x}$ is three dimensional]. We assume that the parameter p is available for external adjustment, and we wish to temporally program our adjustments of p so as to achieve improved performance. We emphasize that our restriction to a three-dimensional system is mainly for ease of presentation, and that the case of higher-dimensional (including infinite-dimensional) systems can be treated by similar methods.[2]

We imagine that the dynamical equations describing the system are not known, but that experimental time series of some scalar-dependent variable $z(t)$ can be measured. Using delay coordinates[3,4] with delay T one can form a delay-coordinate vector,

$$\mathbf{X}(t)=[z(t),z(t-T),z(t-2T),\ldots,z(t-MT)].$$

We are interested in periodic orbits and their stability properties, and we shall use $\mathbf{X}$ to obtain a surface of section for this purpose. In the surface of section, a continuous-time-periodic orbit appears as a discrete-time orbit cycling through a finite set of points. We require the dynamical behavior of the surface of section map in

neighborhoods of these points in order to study the stability of the periodic orbits. To embed a small neighborhood of a point from $\mathbf{x}$ into $\mathbf{X}$, we typically only require as many dimensions as there are coordinates of the point. Thus, for our purposes, $M=D-1$ is generally sufficient. (This is in contrast with[3] $M+1=2D+1$, typically required for global embedding of the original phase space in the delay-coordinate space.) Hence, for the case considered ($D=3$), our surface of section is two dimensional.

We suppose that the parameter p can be varied in a small range about some nominal value p_0. Henceforth, without loss of generality, we set $p_0\equiv 0$. Let the range in which we are allowed to vary p be $p_* > p > -p_*$.

Using an experimental surface of section for the embedding vector $\mathbf{X}$, we imagine that we obtain many experimental points in the surface of section for $p=0$. We denote these points $\xi_1,\xi_2,\xi_3,\ldots,\xi_k$, where ξ_n denotes the coordinates in the surface of section at the nth piercing of the surface of section by the orbit $\mathbf{X}(t)$. For example, a common choice of the surface of section would be $z(t-MT)$ equals a constant, and $\xi_n=[z(t_n),\ldots,z(t_n-(M-1)T)]$, where $t=t_n$ denotes the time at the nth piercing. From such experimentally determined sequences it has been demonstrated that a large number of distinct unstable periodic orbits on a chaotic attractor can be determined.[5,6] We then examine these unstable periodic orbits and select the one which gives the best performance. Again using an experimentally determined sequence, we obtain the stability properties of the chosen periodic orbit (cf. Refs. 5 and 6 for discussion of how this can be done and for descriptions of its implementation in concrete experimental cases). For the purposes of simplicity, let us assume in what follows that this orbit is a fixed point of the surface of section map (i.e., period one; the case of higher period is a straightforward extension). Let λ_s and λ_u be the experimentally determined stable and unstable eigenvalues of the surface of section map at the chosen fixed point of the map ($|\lambda_u|>1>|\lambda_s|$). Let $\mathbf{e}_s$ and $\mathbf{e}_u$ be the experimentally determined unit vectors in the stable and unstable directions. Let $\xi=\xi_F\equiv 0$ be the desired fixed point. We then change p slightly from $p=0$ to some other value $p=\bar{p}$. The fixed-point coordinates in the experimental surface of section will shift from 0 to some nearby point $\xi_F(\bar{p})$ and we determine this new position. For small $\bar{p}$ we approximate $\mathbf{g}\equiv\partial\xi_F(p)/\partial p|_{p=0}\cong\bar{p}^{-1}\xi_F(\bar{p})$, which allows an experimental determination of the vector $\mathbf{g}$.

Thus, in the surface of section, near $\xi=0$, we can use a linear approximation for the map, $\xi_{n+1}-\xi_F(p)\cong\mathbf{M}\cdot[\xi_n-\xi_F(p)]$, where $\mathbf{M}$ is a 2×2 matrix. Using $\xi_F(p)\cong p\mathbf{g}$ we have

$$\xi_{n+1}\cong p_n\mathbf{g}+[\lambda_u\mathbf{e}_u\mathbf{f}_u+\lambda_s\mathbf{e}_s\mathbf{f}_s]\cdot[\xi_n-p_n\mathbf{g}]. \tag{1}$$

[In the linearization (1), we have considered p_n to be small and of the same order as ξ_n.] We emphasize that $\mathbf{g}$, $\mathbf{e}_u$, $\mathbf{e}_s$, λ_u, and λ_s are all experimentally accessible by the embedding technique just discussed. In (1) $\mathbf{f}_u$ and $\mathbf{f}_s$ are contravariant basis vectors defined by $\mathbf{f}_s\cdot\mathbf{e}_s=\mathbf{f}_u\cdot\mathbf{e}_u=1$, $\mathbf{f}_s\cdot\mathbf{e}_u=\mathbf{f}_u\cdot\mathbf{e}_s=0$. Note that we have written the location of the fixed point as $p_n\mathbf{g}$ because we imagine that we adjust p to a new value p_n after each piercing of the surface of section. That is, we observe ξ_n and then adjust p to the value p_n. Thus p_n depends on ξ_n. Further, we only envision making this adjustment when the orbit falls near the desired fixed point for $p=0$.

Assume that ξ_n falls near the desired fixed point at $\xi=0$ so that (1) applies. We then attempt to pick p_n so that ξ_{n+1} falls on the stable manifold of $\xi=0$. That is, we choose p_n so that $\mathbf{f}_u\cdot\xi_{n+1}=0$. If ξ_{n+1} falls on the stable manifold of $\xi=0$, we can then set the parameter perturbations to zero, and the orbit for subsequent time will approach the fixed point at the geometrical rate λ_s. Thus, for sufficiently small ξ_n, we can dot (1) with $\mathbf{f}_u$ to obtain

$$p_n=\lambda_u(\lambda_u-1)^{-1}(\xi_n\cdot\mathbf{f}_u)/(\mathbf{g}\cdot\mathbf{f}_u), \tag{2}$$

which we use when the magnitude of the right-hand side of (2) is less than p_*. When it is greater than p_*, we set $p_n=0$. We assume in (2) that the generic condition $\mathbf{g}\cdot\mathbf{f}_u\neq 0$ is satisfied. Thus, the parameter perturbations are activated (i.e., $p_n\neq 0$) only if ξ_n falls in a narrow strip $|\xi_n^u|<\xi_*$, where $\xi_n^u=\mathbf{f}_u\cdot\xi_n$, and from (2) $\xi_*=p_*|(1-\lambda_u^{-1})\mathbf{g}\cdot\mathbf{f}_u|$. Thus, for small p_*, a typical initial condition will execute a chaotic orbit, unchanged from the uncontrolled case, until ξ_n falls in the strip. Even then, because of nonlinearity not included in (1), the control may not be able to bring the orbit to the fixed point. In this case the orbit will leave the strip and continue to wander chaotically as if there was no control. Since the orbit on the uncontrolled chaotic attractor is ergodic, at some time it will eventually satisfy $|\xi_n^u|<\xi_*$ and also be sufficiently close to the desired fixed point that attraction to $\xi=0$ is achieved. [In rare cases applying Eq. (2) when the trajectory enters the strip, but is still far from 0, may result in stabilizing the wrong periodic orbit which visits the strip.]

Thus, we create a stable orbit, but, for a typical initial condition, it is preceded in time by a chaotic transient in which the orbit is similar to orbits on the uncontrolled chaotic attractor. The length τ of such a chaotic transient depends sensitively on the initial condition, and, for randomly chosen initial conditions, has an exponential probability distribution[7] $P(\tau)\sim\exp[-(\tau/\langle\tau\rangle)]$ for large τ. The average length of the chaotic transient $\langle\tau\rangle$ increases with decreasing p_* and follows a power-law relation[7] for small p_*, $\langle\tau\rangle\sim p_*^{-\gamma}$.

We will now derive a formula for the exponent γ. Dotting the linearized map for ξ_{n+1}, Eq. (1), with $\mathbf{f}_u$, we obtain $\xi_{n+1}^u\cong 0$. In obtaining this result from (1) we have substituted p_n appropriate for $|\xi_n^u|<\xi_*$. We note that the result $\xi_{n+1}^u\cong 0$ is a linearization, and typically

9

has a lowest-order nonlinear correction that is quadratic. In particular, $\xi_{n}^{s}=\mathbf{f}_{s}\cdot\xi_{n}$ is not restricted by $|\xi_{n}^{u}|<\xi_{*}$, and thus may not be small when the condition $|\xi_{n}^{u}|<\xi_{*}$ is satisfied. Hence the correction quadratic in ξ_{n}^{s} is most significant. Including such a correction we have $\xi_{n+1}^{u}\cong\kappa(\xi_{n}^{s})^{2}$, where κ is a constant. Thus, if $|\kappa|(\xi_{n}^{s})^{2}>\xi_{*}$, then $|\xi_{n+1}^{u}|>\xi_{*}$, and attraction to $\xi=0$ is not achieved, even though $|\xi_{n}^{u}|<\xi_{*}$. Attraction to $\xi=0$ is achieved when the orbit falls in the small parallelogram P_{c} given by $|\xi_{n}^{u}|<\xi_{*}$, $|\xi_{n}^{s}|<(\xi_{*}/|\kappa|)^{1/2}$. For very small ξ_{*}, an initial condition will bounce around on the set comprising the uncontrolled chaotic attractor for a long time before it falls in the parallelogram P_{c}. At any given iterate the probability of falling in P_{c} is $\mu(P_{c})$, the measure of the uncontrolled attractor contained in P_{c}. Thus, $\langle\tau\rangle^{-1}=\mu(P_{c})$. The scaling of $\mu(P_{c})$ with ξ_{*} is

$$\mu(P_{c})\sim(\xi_{*})^{d_{u}}[(\xi_{*}/|\kappa|)^{1/2}]^{d_{s}}\sim\xi_{*}^{d_{u}+(1/2)d_{s}},$$

where d_{u} and d_{s} are the partial pointwise dimensions for the uncontrolled chaotic attractor at $\xi=0$ in the unstable direction and the stable direction, respectively. Thus, $\mu(P_{c})=\xi_{*}^{\gamma}$, where $\gamma=d_{u}+d_{s}/2$. Since we assume the attractor to be effectively smooth in the unstable direction, $d_{u}=1$. The partial pointwise dimension in the stable direction is given in terms of the eigenvalues[7] at $\xi=0$, $d_{s}=\ln|\lambda_{u}|/\ln|\lambda_{s}|^{-1}$. Thus,

$$\gamma=1+\tfrac{1}{2}\ln|\lambda_{u}|/\ln|\lambda_{s}|^{-1}. \tag{3}$$

To study the effect of noise we add a term $\epsilon\delta_{n}$ to the right-hand side of the linearized equations for ξ_{n+1}, Eq. (1), where δ_{n} is a random variable and ϵ is a small parameter specifying the intensity of the noise. The quantities δ_{n} are taken to have zero mean ($\langle\delta_{n}\rangle=0$), be independent ($\langle\delta_{n}\delta_{m}\rangle=0$ for $m\neq n$), and have a probability density independent of n. Dotting (1) with noise included with $\mathbf{f}_{u}$ we obtain $\xi_{n+1}^{u}=\epsilon\delta_{n}^{u}$, where $\delta_{n}^{u}\equiv\mathbf{f}_{u}\cdot\delta_{n}$. Thus, if the noise is bounded, $|\delta_{n}^{u}|<\delta_{\max}$, then the stability of $\xi=0$ will not be affected by the noise if the bound is small enough, $\epsilon\delta_{\max}<\xi_{*}$. If this condition is not satisfied, then the noise can kick an orbit which is initially in the parallelogram P_{c} into the region outside P_{c}. We are particularly interested in the case where such kickouts are caused by low-probability tails on the probability density and are thus rare. (If they are frequent, then our procedure is ineffective.) In such a case the average time to be kicked out $\langle\tau'\rangle$ will be long. Thus, an orbit will typically alternate between epochs of chaotic motion of average duration $\langle\tau\rangle$ in which it is far from $\xi=0$, and epochs of average length $\langle\tau'\rangle$ in which the orbit lies in the parallelogram P_{c}. For small enough noise the orbit spends most of its time in P_{c}, $\langle\tau'\rangle\gg\langle\tau\rangle$, and one might then regard the procedure as being effective.

We now consider a specific numerical example. Our purpose is to illustrate and test our analyses of the average time to achieve control and the effect of noise. To do this we shall utilize the Henon map, $x_{n+1}=A-x_{n}^{2}+By_{n}$, $y_{n+1}=x_{n}$, where we take $B=0.3$. We assume that the quantity A can be varied by a small amount about some value A_{0}. Accordingly, we write A as $A=A_{0}+p$, where p is the control parameter. For the values of A_{0} which we investigate, the attractor for the map is chaotic and contains an unstable period-one (fixed-point) orbit. The coordinates (x_{F},y_{F}) of the fixed point which is in the attractor for $p=0$ along with the associated parameters and vectors appearing in Eq. (1) may be explicitly calculated. The quantity ξ_{n} appearing in (1) is $\xi_{n}=(x_{n}-x_{F})\mathbf{x}_{0}+(y_{n}-y_{F})\mathbf{y}_{0}$. To test our prediction for the dependence of $\langle\tau\rangle$, the average time to approach $\xi=0$, on the maximum allowed size of the parameter perturbation p_{*}, we proceed as follows. We iterate the map with $p=0$ using a large number of randomly chosen initial conditions until all these initial conditions are distributed over the attractor (500 iterates were typically used). We then turn on the parameter perturbations and determine for each orbit how many further iterates τ are necessary before the orbit falls within a circle of radius $\frac{1}{2}\xi_{*}$ centered at the fixed point. We then calculate the average of these times. We do this for many different values of p_{*} and plot the results as a function of p_{*}. This is shown on the log-log plot in Fig. 1 along with the theoretical straight line of slope given by the exponent (3). We see that the agreement is

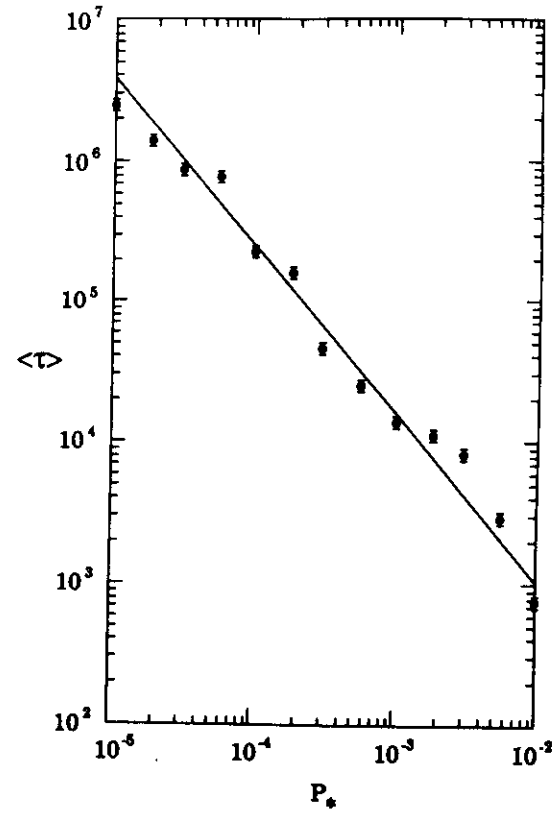

FIG. 1. $\langle\tau\rangle$ vs p_{*}. Points were computed using 128 randomly selected initial conditions. $A_{0}=1.4$.

10

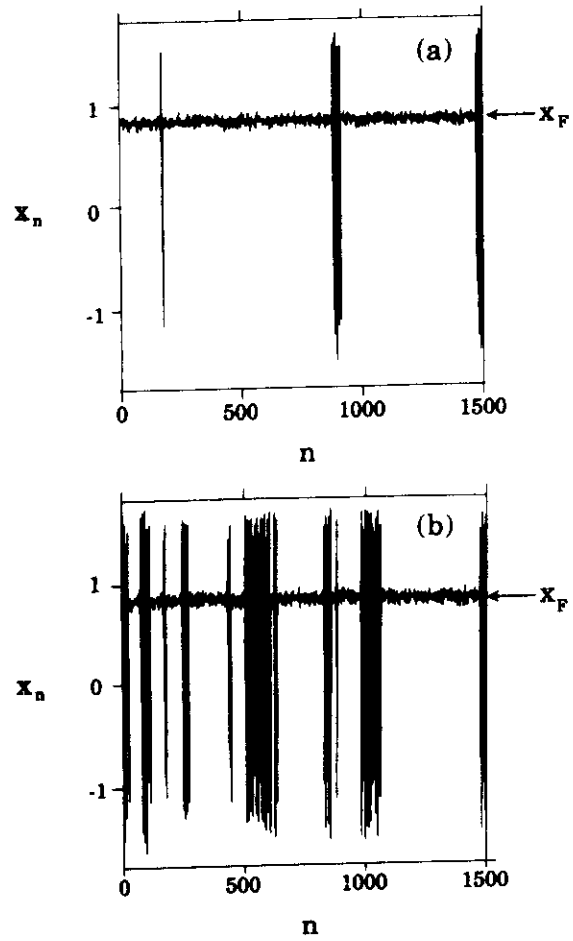

FIG. 2. x_n vs n for two cases with the same realization of the random vector δ. $p_*=0.2$ and $A_0=1.29$ for both cases. (a) $\epsilon=3.5\times10^{-2}$; (b) $\epsilon=3.8\times10^{-2}$.

good although there are significant variations about the general power-law trend. These are to be expected due to the fractal nature of the attractor and have also been seen in numerical calculations of the pointwise dimension for points on chaotic attractors (cf. Grebogi, Ott, and Yorke[1]).

Next, we consider the issue of noise. We add terms $\epsilon\delta_{xn}$ and $\epsilon\delta_{yn}$ to the right-hand sides of the Henon map equations. The random quantities δ_{xn} and δ_{yn} are independent of each other, have mean value 0 and mean-squared value 1 ($\langle\delta_x^2\rangle=\langle\delta_y^2\rangle=1$), and have a Gaussian probability density. Figure 2 shows orbit plots, x_n vs n for 1500 iterates of the noisy map with parameter perturbations given by (2), for two different noise levels and p_* held fixed at $p_*=0.2$. As predicted the orbit stays near the fixed point with occasional bursts into the region far from $\xi=0$, and these bursts are less frequent for small noise levels.

In conclusion, we have shown that there is great inherent flexibility in situations in which the dynamical motion is on a chaotic attractor. In particular, by using only small (carefully chosen) parameter perturbations it is possible to create a large variety of attracting periodic motions and to choose amongst these periodic motions the one most desirable.[8]

This research was supported by the U.S. Department of Energy (Scientific Computing Staff Office of Energy Research). The computation was done at the National Energy Research Supercomputer Center.

---

[a]Laboratory for Plasma Research.
[b]Departments of Electrical Engineering and of Physics.
[c]Institute for Physical Science and Technology and Department of Mathematics.

[1]The periodic orbits are dense in the attractor [i.e., periodic orbits pass through any neighborhood (however small) of any point on the attractor]. For discussions of the relation of ergodic properties of an attractor to its dense set of unstable periodic orbits, see, for example, C. Grebogi, E. Ott, and J. A. Yorke, Phys. Rev. A **37**, 1711 (1988); **36**, 3522 (1987); D. Auerbach *et al.*, Phys. Rev. Lett. **58**, 2387 (1987); H. Hata *et al.*, Prog. Theor. Phys. **78**, 511 (1987); A. Katok, Publ. Math. IHES **51**, 137 (1980); R. Bowen, Trans. Am. Math. Soc. **154**, 377 (1971).

[2]E. Ott, C. Grebogi, and J. A. Yorke, in *Chaos: Proceedings of a Soviet-American Conference* (American Institute of Physics, New York, 1990).

[3]F. Takens, in *Dynamical Systems and Turbulence*, edited by D. Rand and L. S. Young (Springer-Verlag, Berlin, 1981), p. 230.

[4]N. H. Packard *et al.*, Phys. Rev. Lett. **45**, 712 (1980).

[5]G. H. Gunaratne, P. S. Linsay, and M. J. Vinson, Phys. Rev. Lett. **63**, 1 (1989).

[6]D. P. Lathrop and E. J. Kostelich, "The Characterization of an Experimental Strange Attractor by Periodic Orbits" (to be published).

[7]C. Grebogi, E. Ott, and J. A. Yorke, Phys. Rev. Lett. **57**, 1284 (1986); P. Romeiras, C. Grebogi, E. Ott, and J. A. Yorke, Phys. Rev. A **36**, 5365 (1987).

[8]The general problem of controlling chaotic systems, while clearly very important, has, so far, received almost no attention. Two exceptions (which are quite different from our approach) are the papers of Hubler (who typically requires large controlling signals) and Fowler [A. Hubler, Helv. Phys. Acta **62**, 343 (1989); T. B. Fowler, IEEE Trans. Autom. Control **34**, 201 (1989)].

Communicating with Chaos

Scott Hayes[a]
U.S. Army Research Laboratory, Adelphi, Maryland 20783

Celso Grebogi[b],[c] and Edward Ott[b],[d],[e]
University of Maryland, College Park, Maryland 20742
(Received 18 December 1992)

The use of chaos to transmit information is described. Chaotic dynamical systems, such as electrical oscillators with very simple structures, naturally produce complex wave forms. We show that the symbolic dynamics of a chaotic oscillator can be made to follow a desired symbol sequence by using small perturbations, thus allowing us to encode a message in the wave form. We illustrate this using a simple numerical electrical oscillator model.

PACS numbers: 05.45.+b

Much of the fundamental understanding of chaotic dynamics involves concepts from information theory, a field developed primarily in the context of practical communication. Concepts from information theory used in chaos include metric entropy, topological entropy, Markov partitions, and symbolic dynamics [1]. On the other hand, because of their exponential sensitivity, chaotic systems are often said to evolve randomly. This terminology is partially justified if one regards the information obtained by *detailed* observation of the chaotic orbit as being less significant than the statistical properties of the orbits. The object of this Letter is to show that we can use the close connection between the theory of chaotic systems and information theory in a way that is more than purely formal. In particular, we show that the recent realization that chaos can be controlled with *small* perturbations [2] can be utilized to cause the symbolic dynamics of a chaotic system to track a prescribed symbol sequence, thus allowing us to encode any desired message in the signal from a chaotic oscillator. The natural complexity of chaos thus provides a vehicle for information transmission in the usual sense. Furthermore, we argue that this method of communication will often have technological advantages.

Specifically, assume that there is an electrical oscillator producing a large amplitude chaotic signal that one wishes to use for communication. The so-called double scroll electrical oscillator [3] yields a chaotic signal consisting of a seemingly random sequence of positive and negative peaks. If we associate a positive peak with a 1, and a negative peak with a 0, the signal yields a binary sequence. Furthermore, we can use *small* control perturbations to cause the signal to follow an orbit whose binary sequence represents the information we wish to communicate. Hence the chaotic power stage that generates the wave form for transmission can remain simple and efficient (complex chaotic behavior occurs in simple systems), while all the complex electronics controlling the output remains at the low-power microelectronic level.

The basic strategy is as follows. First, examine the free-running (i.e., uncontrolled) oscillator and extract from it a symbolic dynamics that allows one to assign symbol sequences to the orbits on the attractor. Typically, some symbol sequences are never produced by the free-running oscillator. The rules specifying allowed and disallowed sequences are called the *grammar*. Methods for determining the grammar (or an approximation to it) of specific systems have been considered in several theoretical [4] and experimental [5] works. (In the engineering literature, a similar concept exists in the context of constrained communication channels.) The next step is to choose a code whereby any message that can be emitted by the information source can be encoded using symbol sequences that satisfy suitable constraints imposed by the dynamics in the presence of the control. (The construction of codes with such constraints is a standard problem in information theory [6], and will be discussed in the context of communicating with chaos, along with the required generalizations, in a longer paper [7].) The code cannot deviate much from the grammar of the free-running oscillator because we envision using only tiny controls that cannot grossly alter the basic topological structure of the orbits on the attractor. Once the code is selected, the next problem is to specify a control method whereby the orbit can be made to follow the symbol sequence of the information to be transmitted. Finally, the transmitted signal must be detected and decoded.

We now present a simple numerical example illustrating how the preceding strategy is carried out. Figure 1(a) is a schematic diagram of the electrical circuit producing the so-called double scroll chaotic attractor [3]. The nonlinearity comes from a nonlinear negative resistance represented by the voltage v_R in Fig. 1. (Different realizations of the negative resistance are possible; we have constructed one using an operational amplifier circuit, and are designing an experiment using this oscillator to demonstrate information transmission using chaos.) The differential equations describing the double scroll system are

$$C_1\dot{v}_{C_1} = G(v_{C_2} - v_{C_1}) - g(v_{C_1}),$$

$$C_2\dot{v}_{C_2} = G(v_{C_1} - v_{C_2}) + i_L,$$

$$L\dot{i}_L = -v_{C_2}.$$

12

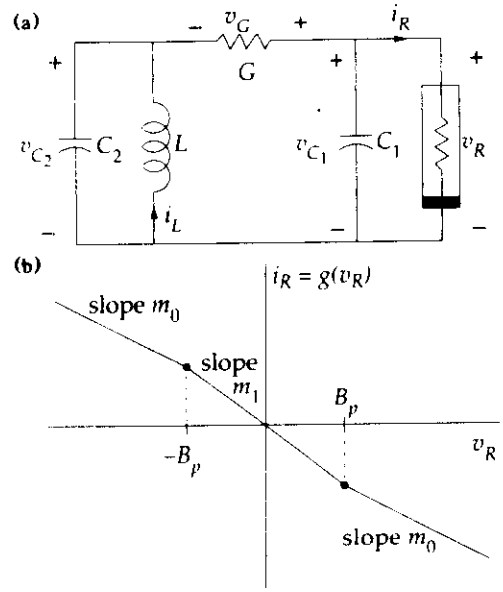

FIG. 1. Double scroll oscillator: (a) electrical schematic and (b) nonlinear negative-resistance i-v characteristic g.

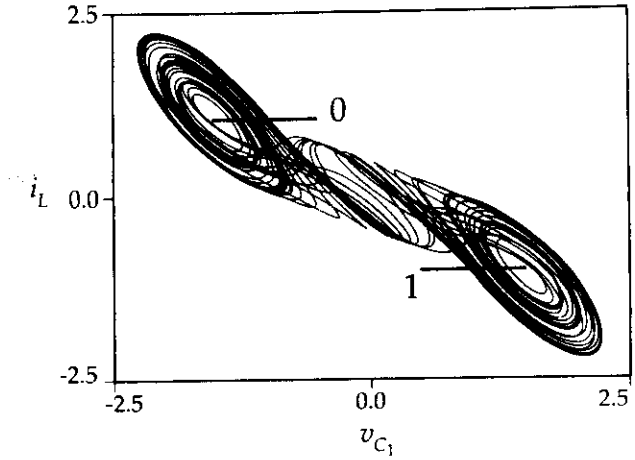

FIG. 2. Double scroll oscillator state-space trajectory projected on the i_L-v_{C_1} plane showing the two branches of the surface of section.

The negative-resistance i-v characteristic g is shown in Fig. 1(b). For our example, we use the normalized parameter values used by Matsumoto [3]: $C_1 = \frac{1}{9}$, $C_2 = 1$, $L = \frac{1}{7}$, $G = 0.7$, $m_0 = -0.5$, $m_1 = -0.8$, and $B_p = 1$. For a Poincaré surface of section (see Fig. 2), we take the surfaces $i_L = \pm GF$, $|v_{C_1}| \leq F$, where $F = B_p(m_0 - m_1)/(G + m_0)$, so that these half planes intersect the attractor with edges at the unstable fixed points at the center of the attractor lobes. Figure 2 shows a trajectory of the double scroll system with the two branches of the surface of section labeled 0 and 1. (The plane surfaces are edge-on in the picture.) The intersection of the strange attractor with the surface of section is approximately a single straight line segment on each of the two branches. Let x denote the distance along this straight line segment from the fixed point at the center of the respective lobe, $x = (F - |v_{C_1}|)\cos\theta + |v_{C_2}|\sin\theta$, where θ is the angle that the line segment makes with the i_L-v_{C_1} plane. Because absolute values are used in defining x, we can use the same x coordinate for both lobes of the attractor.

To construct a description of the symbolic dynamics of the system, we run the computer simulation without control. When the free-running system state point passes through the surface of section, we record the value of the generalized coordinate x (restricted to 1000 discrete bins for the computer simulation), and then record the symbol sequence that is generated by the system after the state point crosses through the surface. Suppose the system generates the binary symbol sequence $b_1 b_2 b_3 \ldots$. We represent this by the real number $0.b_1 b_2 b_3 \ldots$, so that each symbol sequence corresponds to the real number $r = \sum_{n=1}^{\infty} b_n 2^{-n}$, and symbols that occur at earlier times are given greater weight. We refer to the number r, specifying the future symbol sequence, as the *symbolic state* of the system. This defines a function mapping the state-space coordinate x on the surface of section to the symbolic coordinate r. This function $r(x)$ (which we call the *coding function*) is shown in Fig. 3. (The function gives actual symbol sequences when referring to the 0 lobe, and the bitwise complement when referring to the 1 lobe.) Because the oscillator is only approximately described by a binary sequence, multiple values of x lead to the same future symbol sequence. (We only need to track one of them. More sophisticated techniques both for symbol assignment and symbol sequence ordering are discussed in the longer paper [7].) Because the intersection of the attractor with the surface of section is only approximately one dimensional, there is a slight uncertainty in the symbolic state for some values of x; this uncertainty is indicated by the shading in the regions between the upper and lower bounds on the value of r in Fig. 3. Observations of the time wave form produced by the oscillator suggest that the grammar is simple: Any sequence of

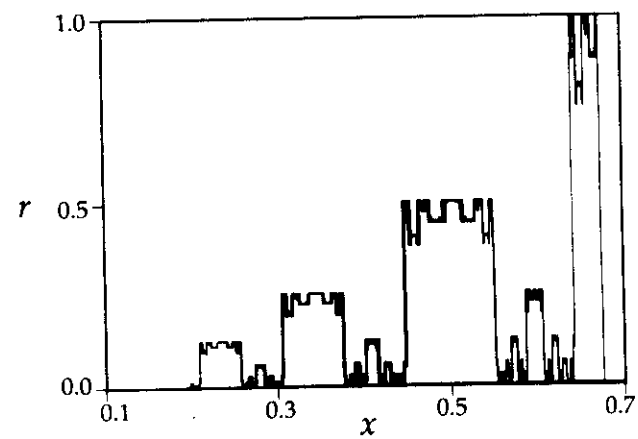

FIG. 3. Binary coding function $r(x)$ for the double scroll system.

19

binary symbols is allowed, except there can never be less than two oscillations of the same polarity. (We do not discuss the full grammar here, but instead adopt this simple grammar for simplicity of description.) This no-single-oscillation rule leads to a very simple coding: Insert an extra 1 after every block of 1's in the binary stream to be transmitted, and an extra 0 after every block of 0's. This altered data stream now satisfies the constraints of the grammar, and is uniquely decodable: Simply remove a 1 from every block of 1's upon reception, and a 0 from every block of 0's. Thus k oscillations of a given polarity represent $k-1$ information bits.

We now discuss how we control the system to follow a desired binary symbol sequence. Say the system state point passes through branch 0 of the surface of section (shown in Fig. 2) at $x=x_a$, and next crosses the surface of section (on either branch 0 or 1) at $x=x_b$. Because we have previously determined the function $r(x)$, we can use the stored values to find the symbolic state $r(x_a)$. We then convert the number $r(x_a)$ to its corresponding binary sequence truncated at some chosen length N, and store this finite-length symbol sequence in a *code register*. As the system state point travels towards its next encounter with the surface of section at $x=x_b$, we shift the sequence in the code register left, discarding the most significant bit (the leftmost bit), and insert the first desired information code bit in the now empty least significant slot (the rightmost slot) of the code register. We then convert this new symbol sequence to its corresponding symbolic state r_b'. Now, when the system state point crosses the surface of section at $x=x_b$, we use a simple search algorithm to find the nearest value of the coordinate x that corresponds to the desired symbolic state r_b'; call this x_b'. By construction, $|r(x_b)-r(x_b')| \leq 2^{-N}$. [If $r(x)$ is continuous, as in the Lorenz system, for example, this search can be replaced by a more efficient local derivative projection to find the desired value of x.] Now let $\delta x = x_b - x_b'$. Because we have chosen the branches of the surface of section at constant values of the inductor current i_L, the deviation δx in the generalized coordinate corresponds to a deviation in the voltages v_{C_1} and v_{C_2} across the two capacitors in Fig. 1. We thus apply a vector correction parallel to the surface of section (at constant i_L) along the attractor cross section to put the orbit at $x=x_b'$. This small correcting voltage perturbation is given by $\delta v_{C_1} = \pm \delta x \cos(\theta)$, $\delta v_{C_2} = \pm \delta x \sin(\theta)$, where the + signs are used for lobe 1 of the attractor, and the − signs for lobe 0. We plan to do this experimentally with current pulse generators connected in parallel with each capacitor. (Many methods of applying control perturbations are possible, but this one is particularly straightforward.) On each successive pass through the surface of section, a new code bit is shifted into the code register, and we repeat the procedure to correct the state-space coordinates, and thus the symbolic state, of the system. The coded information sequence, because it is shifted through the code register, does not begin to appear in the output wave form until N iterations of the procedure, where N is the length of the code register. If the symbol sequence is coming from a properly coded discrete ergodic information source, the process of shifting the information sequence through the code register can be viewed as locking the symbolic dynamics of the oscillator to the information source. Thus, there is a short transient phase during which the symbolic dynamics of the oscillator is being locked to the information source, and the symbolic dynamics of the oscillator is always N bits behind the information source.

Figure 4 shows an encoded wave form for the double scroll system produced by the described technique. This wave form corresponds to the voltage wave form $v_G(t)$ across the passive conductance G. If the conductance G is replaced by a transmission channel of the same impedance, the signal produced can be transmitted through the channel. We have represented each letter of the Roman alphabet by the five-bit binary number for its location in the alphabet, and added the extra bits to satisfy the no-single-oscillation constraint to encode the word "chaos." We have applied the technique to first bring the system to a periodic orbit about lobe 1 of the attractor, then to execute the writing of the word, and then to bring the system back to a periodic orbit about lobe 0. The trajectory shown in Fig. 2 is actually the encoded trajectory, but this is not apparent in the figure because the controlled trajectory approximates a possible natural trajectory. The root-mean-squared amplitude of the control signal over the writing of the word was of order 10^{-3} in the normalized units. The control probably cannot be made much smaller using this simple technique, primarily because the one-dimensional approximation in the surface of section causes the coding function to be slightly inaccurate. This control amplitude, though already very small compared to the oscillator signal voltages, does not

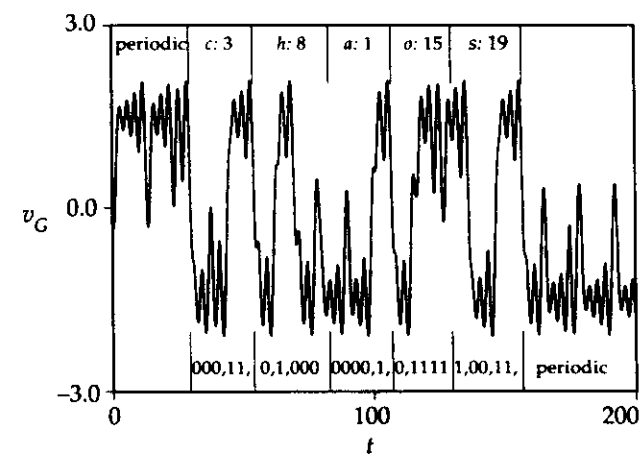

FIG. 4. Controlled $v_G(t)$ signal for the double scroll system encoded with "chaos." Each letter is shown at the top of the figure, along with its numerical position in the alphabet. Shown at the bottom are the corresponding binary code words. Extra bits (indicated by commas) are added to satisfy the constraints imposed by the grammar.

14

appear to be a fundamental limit, and we are developing control techniques to reduce it.

We conclude with some comments concerning the scope, application, and theoretical significance of our technique.

(1) Since we envision the transmitted signal to be a single scalar, its instantaneous value does not specify the full system state of the chaotic oscillator. If more state information is needed to extract the symbol sequence, time delay embedding [8] can be used. As our example using the double scroll equations shows, however, time delay embedding is not always necessary.

(2) Because our control technique uses only small perturbations [9], the dynamical motion of the system is approximately described by the equations for the uncontrolled system. Knowing the equations of motion greatly simplifies the task of removing noise [10] from a received signal. The basic bipolar nature of the signal in Fig. 4 implies that the message can still be extracted for noise amplitudes that are significant, but not too large compared to the signal. We consider the effects of additive noise on the detection of chaos signals quantitatively in the longer paper [7].

(3) Signals that are generated by chaotic dynamical systems and carry information in their symbolic dynamics have an interesting and possibly useful property: More than one encoded symbol can be extracted from a single sample of the trajectory if time delay embedding is used. This is done by using the state-space partition for a higher order iterate of the return map [7] of the system.

(4) Much of the theory needed to understand information transmission using the symbolic dynamics of chaotic systems already exists [11]. For example, because the topological entropy [12] of a dynamical system is the asymptotic growth exponent of the number of finite symbol sequences that the system can generate (given the best state-space partition), the channel capacity of a chaotic system used for information transmission is given by the topological entropy. The types of channel constraints that arise with a chaotic system will be discussed in a longer paper [7], along with other theoretical considerations.

(5) We emphasize that the particular methods for control and coding used in our double scroll example were chosen for simplicity, and that other more optimal methods are possible. Also, the double scroll oscillator itself was chosen because it is simple, and a large body of research is available about its dynamics. It is not intended as an example of a practical oscillator for communication wave form synthesis. It may be possible to use a higher-dimensional radio-frequency band-limited chaotic system for improved performance (higher information rate and better noise immunity), roughly analogous to the use of complex signaling constellations in classical communication systems. We are now developing more practical high-speed symbolic control techniques that could be used at higher bit rates than an implementation of the straightforward example given here.

(6) There has been much discussion of the role of chaos in biological systems, and we speculate that the control of chaos with tiny perturbations may be important for information transmission in nature.

This research was supported by Harry Diamond Laboratories (now the U.S. Army Research Laboratory), and by the U.S. Department of Energy (Office of Scientific Computing, Office of Energy Research).

---

[a]Also at Department of Physics and Astronomy, University of Maryland, College Park, MD 20742.
[b]Laboratory for Plasma Research.
[c]Institute for Physical Science and Technology and Department of Mathematics.
[d]Department of Physics and Astronomy.
[e]Department of Electrical Engineering.

[1] For a pedagogical discussion emphasizing the role of concepts from information theory in chaos, see R. Shaw, Z. Naturforsch. **36A**, 80 (1981).

[2] (a) E. Ott, C. Grebogi, and J. A. Yorke, Phys. Rev. Lett. **64**, 1196 (1990); (b) T. Shinbrot, E. Ott, C. Grebogi, and J. A. Yorke, Phys. Rev. Lett. **65**, 3215 (1990).

[3] Several articles about this circuit appear in Proc. IEEE **75**, No. 8 (1987): e.g., T. Matsumoto, p. 1033.

[4] P. Cvitanović, G. Gunaratne, and I. Procaccia, Phys. Rev. A **38**, 1503 (1988); P. Grassberger, H. Kantz, and U. Moenig, J. Phys. A **22**, 5217 (1989).

[5] D. P. Lathrop and E. J. Kostelich, Phys. Rev. A **40**, 4028 (1989); L. Flepp, R. Holzner, E. Brun, M. Finardi, and R. Badii, Phys. Rev. Lett. **67**, 2244 (1991).

[6] R. E. Blahut, *Principles and Practice of Information Theory* (Addison-Wesley, Reading, MA, 1988); C. E. Shannon and W. Weaver, *The Mathematical Theory of Communication* (University of Illinois Press, Chicago, 1963).

[7] S. Hayes, C. Grebogi, and E. Ott (to be published).

[8] F. Takens, in *Dynamical Systems and Turbulence*, edited by D. A. Rand, Springer Lecture Notes in Mathematics Vol. 898 (Springer-Verlag, New York, 1981), p. 366.

[9] Our control technique can also be used to target a chaotic system [2(b)] in state space. The relationship between symbolic states and state-space coordinates is established by the coding function $r(x)$.

[10] E. J. Kostelich and J. A. Yorke, Phys. Rev. A **38**, 1649 (1988); S. M. Hammel, Phys. Lett. A **148**, 421 (1990). It is easier to filter noise that is introduced in the communication channel than it is to filter noise that is present in the chaotic oscillator itself.

[11] A very different concept is that of using the synchronization of two chaotic systems [L. M. Pecora and T. L. Carroll, Phys. Rev. Lett. **64**, 821 (1990)] for secure communications. In this case a small information-bearing signal is masked by a large chaotic signal. Several papers discussing this appear in *Proceedings of the International Conference on Acoustics, Speech, and Signal Processing* (IEEE, New York, 1992). This mechanism is not, however, based on the information theoretic formalism of chaos.

[12] R. L. Adler, A. G. Konheim, and M. H. McAndrew, Trans. Am. Math. Soc. **114**, 309 (1965).

Plateau Onset for Correlation Dimension: When Does it Occur?

Mingzhou Ding,[1] Celso Grebogi,[2,3] Edward Ott,[2,4] Tim Sauer,[5] and James A. Yorke[3]

[1]*Center for Complex Systems and Department of Mathematics, Florida Atlantic University, Boca Raton, Florida 33431*

[2]*Laboratory for Plasma Research, University of Maryland, College Park, Maryland 20742*

[3]*Department of Mathematics and Institute for Physical Science and Technology, University of Maryland, College Park, Maryland 20742*

[4]*Departments of Physics and of Electrical Engineering, University of Maryland, College Park, Maryland 20742*

[5]*Department of Mathematical Sciences, George Mason University, Fairfax, Virginia 22030*

(Received 22 February 1993)

Chaotic experimental systems are often investigated using delay coordinates. Estimated values of the correlation dimension in delay coordinate space typically increase with the number of delays and eventually reach a plateau (on which the dimension estimate is relatively constant) whose value is commonly taken as an estimate of the correlation dimension D_2 of the underlying chaotic attractor. We report a rigorous result which implies that, for long enough data sets, the plateau begins when the number of delay coordinates first exceeds D_2. Numerical experiments are presented. We also discuss how lack of sufficient data can produce results that seem to be inconsistent with the theoretical prediction.

PACS numbers: 05.45.+b

The estimation of the correlation dimension [1] of a presumed chaotic time series has been widely used by scientists to assess the nature of a variety of experimental as well as model systems, ranging from simple circuits to chemical reactions to the human brain. It is also known that many factors, such as noise and a lack of data, can hinder the successful application of the dimension extraction algorithm. In this paper, we address two issues related to the understanding of these difficulties, namely, what happens in an ideal situation (i.e., long data string with low noise) and what could be expected when the data set is small. In particular, we focus on the character of the dependence of the estimated correlation dimension on the dimension of the delay coordinate reconstruction space.

Consider an n-dimensional dynamical system that exhibits a chaotic attractor. A correlation integral $C(\epsilon)$ [1] is defined to be the probability that a pair of points chosen randomly on the attractor with respect to the natural measure ρ is separated by a distance less than ϵ on the attractor. The correlation dimension D_2 [1] of the attractor is then defined as $D_2 = \lim_{\epsilon \to 0} \log C(\epsilon)/\log \epsilon$. Assume that we measure and record a trajectory of finite duration L on the attractor at N equally spaced discrete times, $\{\mathbf{x}_i\}_{i=1}^{N}$, where $\mathbf{x}_i \in \mathbf{R}^n$. The correlation integral $C(\epsilon)$ is then approximated by

$$C(N,\epsilon) = \frac{2}{N(N-1)} \sum_{j=1}^{N} \sum_{i=j+1}^{N} \Theta(\epsilon - |\mathbf{x}_i - \mathbf{x}_j|), \quad (1)$$

where $\Theta(x) = 1$ for $x > 0$ and $\Theta(x) = 0$ for $x \leq 0$. In the limit $L, N \to \infty$, $C(N,\epsilon) \to C(\epsilon)$.

The dynamical information of a chaotic experimental system is often contained in a time series, $\{y_i = y(t_i)\}_{i=1}^{N}$, obtained by measuring a single scalar function $y = h(\mathbf{x})$ where $\mathbf{x} \in \mathbf{R}^n$ is the original phase space variable. From $\{y_i\}_{i=1}^{N}$ one reconstructs an m-dimensional vector $\mathbf{y}_i$ using the delay coordinates [2,3]

$$\mathbf{y}_i = \{y(t_i), y(t_i - T), \ldots, y(t_i - (m-1)T)\}, \quad (2)$$

where $T > 0$ is the delay time and m is the dimension of the reconstruction space. We call the mapping from $\{\mathbf{x}_i\}$ in $\mathbf{R}^n$ to $\{\mathbf{y}_i\}$ in $\mathbf{R}^m$ the "delay coordinate map." Results in Ref. [4] show that, for typical $T > 0$ and $m > 2D_0$, this delay coordinate map is one to one. Here D_0 is the box-counting dimension of the original chaotic attractor.

Our main focus is to estimate correlation dimension from a time series using delay coordinates [Eq. (2)]. As a point of departure for subsequent discussions, we first report a theorem [5,6] which shows that, for estimating the correlation dimension, $m \geq D_2$ suffices. We emphasize that this result holds true irrespective of whether the delay coordinate map is one to one or not. This is contrary to the commonly accepted notion that an embedding (one to one and differentiable) is needed for dimension estimation, leading to the false surmise that m needs to be at least $2D_2 + 1$ to guarantee a correct dimension estimation (see [7] for further discussion).

Consider an n-dimensional map $G: \mathbf{R}^n \to \mathbf{R}^n$. Let A be an attractor of G in $\mathbf{R}^n$ with a natural probability measure ρ. For a function $h: \mathbf{R}^n \to \mathbf{R}$, define a delay coordinate map $F_h: \mathbf{R}^n \to \mathbf{R}^m$ as

$$F_h(\mathbf{x}) = [h(\mathbf{x}), h(G^{-1}(\mathbf{x})), \ldots, h(G^{-(m-1)}(\mathbf{x}))].$$

The projected image of the attractor A under F_h has an induced natural probability measure $F_h(\rho)$ in $\mathbf{R}^m$. Furthermore, assume that G has only a finite number of periodic points of period less than or equal to m in A. The following result then applies.

Theorem.—If $D_2(\rho) \leq m$, then for almost every h, $D_2(F_h(\rho)) = D_2(\rho)$.

The theorem says that the correlation dimension is preserved under the delay coordinate map with $m \geq D_2(\rho)$. Similar results hold for flows generated by ordinary differential equations. "Almost every" in the statement is understood in the sense of prevalence defined in Ref. [4]; roughly speaking, we can regard this "almost every" as meaning that the functions h that do not give

0031-9007/93/70(25)/3872(4)$06.00

the stated result are very scarce and are not expected to occur in practice. The above dimension preservation result also holds for almost all general projection maps meeting the condition in the theorem. To illustrate, consider a closed curve with a uniform measure in $\mathbf{R}^3$. The dimension of this curve is 1. The projected image of this curve onto the plane still has a dimension of 1 but is generally self-intersecting. Thus the map is not one to one but preserves dimension information. One can further project the image to $\mathbf{R}^1$ and obtain an interval, which again has a dimension of 1 but bears little resemblance to the original curve in $\mathbf{R}^3$.

In applications D_2 is commonly extracted from a time series as follows (see Refs. [8–11] for reviews). First, an m-dimensional trajectory is constructed using Eq. (2). Then, the correlation integral $C_m(N,\epsilon)$ is computed according to Eq. (1), where m indicates the dimensionality of the reconstruction space. From the curve $\log C_m(N,\epsilon)$ vs $\log\epsilon$ one then locates a linear scaling region for small ϵ and estimates the slope of the curve over the linear region. This slope, denoted $\bar{D}_2^{(m)}$, is then taken as an estimate of the correlation dimension $D_2^{(m)}$ of the projection of the attractor to the m-dimensional reconstruction space. If these estimates $\bar{D}_2^{(m)}$, plotted as a function of m, appear to reach a plateau for a range of large enough m values, then we denote the plateaued value $\bar{D}_2$ and take $\bar{D}_2$ an estimate of the true correlation dimension D_2 for the system. From the theorem it is clear that the onset of this plateau should ideally start at $m = \mathrm{Ceil}(D_2)$, where $\mathrm{Ceil}(D_2)$, standing for ceiling of D_2, denotes the smallest integer greater than or equal to D_2.

Our original interest in the current problem was motivated by published reports (see Refs. [12–17] for a sample) where $\bar{D}_2^{(m)}$ plateaus at m values that are considerably greater than $\bar{D}_2$. A particular concern is that, when this happens, what does it imply regarding the correctness of the assertion that $\bar{D}_2$ is an estimate of the true correlation dimension D_2 of the underlying chaotic process? In an attempt to answer this question we have obtained new results on the systematic behavior of the correlation integrals. Based on these behaviors we are able to explain how factors such as a lack of sufficient data can produce results, resembling those seen in the experimental reports cited above, which seem to be inconsistent with the theorem. Furthermore, we find that even in cases where the plateau onset of $\bar{D}_2^{(m)}$ occurs at m values considerably greater than $\mathrm{Ceil}(\bar{D}_2)$, there are situations where the plateaued $\bar{D}_2$ is a good estimate of the true correlation dimension D_2. See Refs. [18–25] for other relevant works addressing the issue of short data sets and noise.

To study the numerical aspects of dimension estimation we use chaotic time series generated by the Mackey-Glass equation [26] $dy(t)/dt = ay(t-\tau)/\{1+[y(t-\tau)]^{10}\} - by(t)$, where we fix $a=0.2$, $b=0.1$, $c=10.0$, and $\tau=100.0$, and take as the initial condition $y(t)=0.5$ for $t \in [-\tau,0]$. The numerical integration of this equation is done by the following iterative scheme [1]:

$$y(t+\delta t) = \frac{2-b\delta t}{2+b\delta t}y(t) + \frac{\delta t}{2+b\delta t}\left\{\frac{ay(t-\tau)}{1+[y(t-\tau)]^{10}} + \frac{ay(t-\tau+\delta t)}{1+[y(t-\tau+\delta t)]^{10}}\right\}, \tag{3}$$

where δt is the integration step size. We choose $\delta t = 0.1$. Equation (3) is then a 1000-dimensional map, which, aside from being an approximation to the original equation, is itself a dynamical system. The time series, generated with a sampling time $t_s = 10.0$, are normalized to the unit interval so that the reconstructed attractor lies in the unit hypercube in the reconstruction space. The norm we use to calculate distances in Eq. (1) is the max-norm in which the distance between two points is the largest of all the component differences. To reconstruct the attractor, we follow Eq. (2) and take the delay time to be $T = 20.0$ The dimension of the reconstruction space is varied from $m = 2$ to $m = 25$.

The first time series, used to illustrate the theorem, consists of 50000 points. For each reconstructed attractor at a given m we calculate the correlation integral $C_m(N,\epsilon)$ according to Eq. (1). In Fig. 1 we display $\log_2 C_m(N,\epsilon)$ vs $\log_2\epsilon$ for $m = 2$–8, 11, 15, 19, 23. For each m we identify a scaling region for small ϵ and fit a straight line through the region. The open circles in Fig. 2 show the values of $\bar{D}_2^{(m)}$ so estimated as a function of m. For $m \leq 7$, $\bar{D}_2^{(m)} \approx m$. For $m \geq 8$, $\bar{D}_2^{(m)}$ plateaus at $\bar{D}_2$ which has a value of about 7.1. Identifying $\bar{D}_2$ with the true correlation dimension D_2 of the underlying attractor, this result is consistent with the prediction by the theorem that the onset of the plateau occurs at $m = \mathrm{Ceil}(D_2)$.

The second time series, used to illustrate the effect

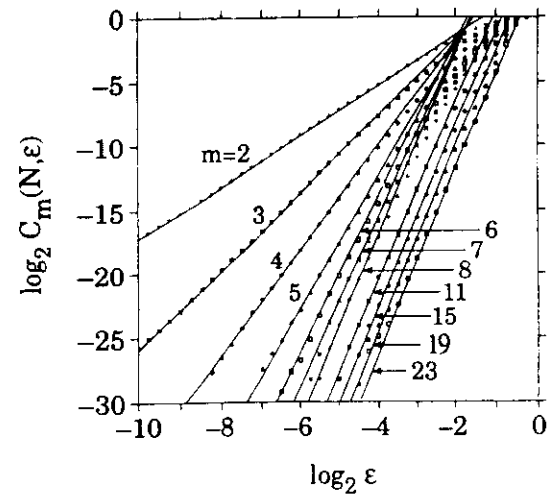

FIG. 1. Log-log plots of the correlation integrals $C_m(N,\epsilon)$ for the data set of 50000 points generated by Eq. (3).

17

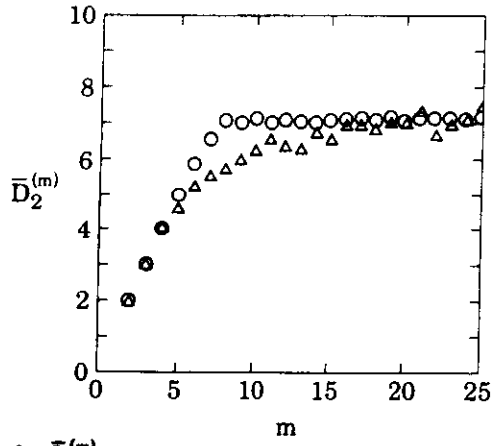

FIG. 2. $\bar{D}_2^{(m)}$ vs m plotted as open circles for the long data set ($N=50000$ and Fig. 1), $\bar{D}_2^{(m)}$ vs m plotted as triangles for the short data set ($N=2000$ and Fig. 3).

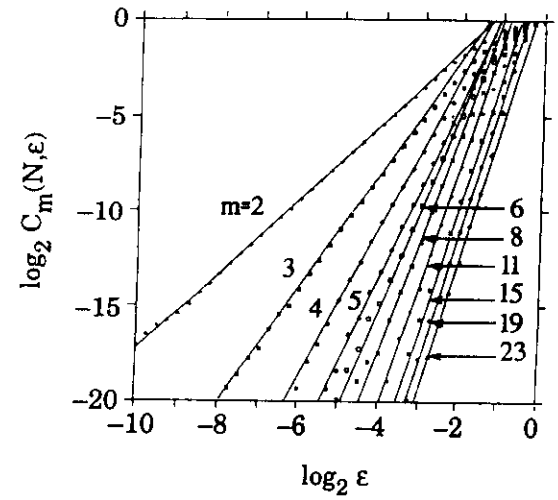

FIG. 3. $\log_2 C_m(N,\epsilon)$ vs $\log_2\epsilon$ for the data set of 2000 points.

due to a lack of data, consists of 2000 points. The $\log_2 C_m(N,\epsilon)$ vs $\log_2\epsilon$ curves are shown in Fig. 3 for $m=2$–6, 8, 11, 15, 19, 23. The values of $\bar{D}_2^{(m)}$ in this case are plotted using triangles as a function of m in Fig. 2. This function attains an approximate plateau which begins at $m=16$ and extends beyond $m=25$. The slope averaged over the plateau is about 7.05 which is consistent with the value of 7.1 obtained using the long data set ($N=50000$) plotted as open circles in Fig. 2. But the D_2 estimates for the short data set fall systematically under that for the long data set for $5 \le m \le 13$. Thus the plateau does not begin until m is substantially larger than Ceil($\bar{D}_2$). This behavior has also been seen in many experimental studies. In what follows we explain the origin of this apparent inconsistency by exploring the systematic behavior of correlation integrals.

Figure 4 is a schematic diagram of a set of correlation integrals for $m=2$ to $m=13$. A dashed line is fit through the scaling region for each m. For $m \le 5$, $\bar{D}_2^{(m)} \approx m$. For $m \ge 6$, $\bar{D}_2^{(m)}$ plateaus at $\bar{D}_2 \approx 5.7$. This value is an estimate of the true D_2 for the system. This figure exhibits several features that are typical of correlation integrals for chaotic systems. The first feature we note is that the horizontal distance between $\log C_m(N,\epsilon)$ and $\log C_{m+1}(N,\epsilon)$ for $m \ge 6$ in the scaling regions is roughly a constant. This constant is predicted, for large m and small ϵ, to be $\Delta h = \Delta v/D_2$, where $\Delta v = TK_2$ with K_2 the correlation entropy [27] and T the delay time in Eq. (2). Two other significant features exhibited by Fig. 4 are as follows. For $m \le 9$, $\log_2 C_m(N,\epsilon)$ increases with a gradually diminishing slope; while for $m \ge 11$, after exiting the linear region, the log-log plots in Fig. 4 first increase with a slope that is steeper than that in the linear scaling region and then level off to meet the point (0,0). These two different trends give rise to an uneven distribution in the extent of the scaling regions for different m with the most extended scaling region occurring at $m=10$.

In Refs. [8,28] arguments are presented to show that the trend observed for relatively small m is due to an "edge effect" resulting from the finite extent to the reconstructed attractor. Ding *et al.* [5] show that the steeper slope observed for relatively large m is caused by foldings occurring on the original attractor. This can be illustrated analytically [5] for the tent map [29]. For $m=1$, the correlation integral for the reconstructed tent map attractor is $C_1(\epsilon)=\epsilon(2-\epsilon)$. For $m=2$, $C_2(\epsilon)$ is written as $C_2(\epsilon)=C_1(\epsilon/2)+R(\epsilon)$. The first term arises because a pair of points y_j and y_l in the time series satisfying $|y_j-y_l|<\epsilon/2$ give rise to a pair of two-dimensional points, $\mathbf{y}_{j+1}=\{y_{j+1},y_j\}$ and $\mathbf{y}_{l+1}=\{y_{l+1},y_l\}$, satisfying $|\mathbf{y}_{j+1}-\mathbf{y}_{l+1}|<\epsilon$. The folding of the tent map at $y=\frac{1}{2}$ leads to situations in which $|y_j-y_l|>\epsilon/2$, but $|y_{j+1}-y_{l+1}|<\epsilon$. Thus the folding in the attractor underlies the correction term $R(\epsilon)$ which is calculated [5] to be $R(\epsilon)=\epsilon^2/2$ for $0 \le \epsilon < \frac{1}{3}$ and $R(\epsilon)=3\epsilon-7\epsilon^2/4-1$ for $\frac{1}{3} \le \epsilon \le 1$. For $0 \le \epsilon < \frac{1}{3}$, $d\log_2 C_2(\epsilon)/d\log_2\epsilon = 1+\epsilon/(2+\epsilon)$. This derivative is 1 when $\epsilon=0$ ($D_2=1$ for the attractor) and increases due to the term $\epsilon/(2+\epsilon)$ whose presence reflects the influence of $R(\epsilon)$ which, in turn, is caused by the folding on the attractor.

From Eq. (1), the range of $C_m(N,\epsilon)$ is $\log_2 2/N^2$

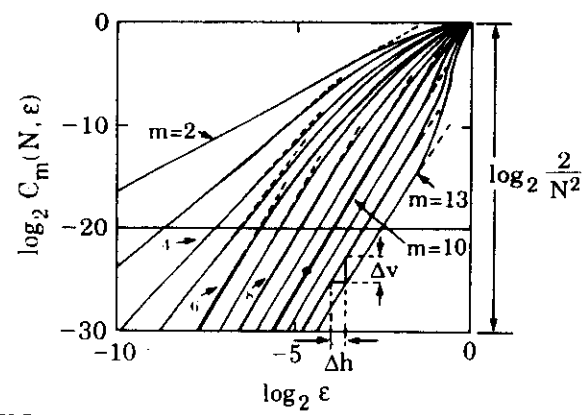

FIG. 4. Schematic diagram of correlation integrals.

18

$\leq \log_2 C_m(N,\epsilon) \leq 0$. Imagine a time series of $N=2000$ points generated by the system underlying Fig. 4. The plots of $\log_2 C_m(N,\epsilon)$ vs $\log_2\epsilon$ for this data set roughly correspond to the portion of Fig. 4 above the horizontal line drawn at $\log_2 C_m(N,\epsilon) = \log_2[2/(2000)^2] \approx -20$. Since the upper boundary points of the scaling regions for $m=6$ and 7 are under this horizontal line, the correct dimension is not obtained for $m=6$ and 7. In fact, if we fit a straight line to an *apparent* linear region above $\log_2 C_m(N,\epsilon) = -20$ for $m=6$ we obtain a slope which is markedly smaller than the actual dimension. However, since the upper boundary points of the scaling regions for $m \geq 8$ are above the horizontal line, we can still expect to obtain the correct estimate of $D_2=5.7$ for $m \geq 8$. Thus the plateau onset is delayed due to a lack of data.

The same consideration applies to the short data set generated by Eq. (3). In particular, imagine that we restrict our attention to the region $\log_2 C_m(N,\epsilon) > -20$ in Fig. 1 and fit a line through an *apparent* linear range for the $m=8$ data in this region. The slope of this straight line is about 5.9, which is roughly the same as that of 5.8 estimated using 2000 points. Thus, by knowing the correlation integrals for a large data set, we can roughly predict the outcome of a dimension measurement based on a smaller subset of this data.

We remark that if one extends the range of m values beyond what is shown in Fig. 2, at large enough m, $\bar{D}_2^{(m)}$ will start to deviate from the plateau behavior and increase monotonically with m. This is caused by the finite length of the data set and can be understood from the systematic behavior of correlation integrals seen in Fig. 4. A lack of sufficient data will not only delay the plateau onset, but also make the deviation from the plateau behavior occur at smaller values of m, thus shortening the plateau length from both sides. This can again be understood with reference to Fig. 4.

This work was supported by the U.S. DOE (Office of Scientific Computing, Office of Energy Research) and the NSF (Divisions of Mathematical and Physical Sciences). M.D.'s research is also supported in part by a grant from the National Institute of Mental Health.

[1] P. Grassberger and I. Procaccia, Phys. Rev. Lett. **50**, 346 (1983); Physica (Amsterdam) **9D**, 189 (1983).
[2] J.-P. Eckmann and D. Ruelle, Rev. Mod. Phys. **57**, 617 (1985).
[3] F. Takens, in *Dynamical Systems and Turbulence*, edited by D. Rand and L. S. Young (Springer-Verlag, Berlin, 1981), p. 366; R. Mañe, *ibid.*, p. 230.
[4] T. Sauer, J. A. Yorke, and M. Casdagli, J. Stat. Phys. **65**, 579 (1991).
[5] M. Ding, C. Grebogi, E. Ott, T. Sauer, and J. A. Yorke, Physica (Amsterdam) D (to be published).
[6] T. Sauer and J. A. Yorke (to be published).
[7] To get a rough idea of how widespread the misconception about the relevance of embedding to dimension estimation is, we conducted a literature search using the Science Citation Index for the years from 1987 to 1992 by looking for papers citing both Ref. [1] and Ref. [3]. We found 183 such papers. We then randomly selected a sample of 22 of these papers for closer examination. The following is what we found. Among the 22 papers there are 15 of them that calculate correlation dimension from time series. Five of these 15 papers make explicit connections between $2D+1$ and dimension estimation. The rest of these papers ignore this issue entirely. Based on this information we estimate that, during the period from 1987 to 1992, there are at least 42 papers (probably many more) where the authors implicitly or explicitly assumed that a one-to-one embedding is needed for dimension calculation. In addition, among the papers we researched for this work, only [8] and [9] imply that $m \geq D_2$ is sufficient for estimating D_2, although no justification is given.
[8] J. Theiler, J. Opt. Soc. Am. A **7**, 1055 (1990).
[9] P. Grassberger, in *Chaos*, edited by A. V. Holden (Manchester Univ. Press, Manchester, 1986).
[10] P. Grassberger, T. Schreiber, and C. Schaffrath, Int. J. Bifurcation Chaos **1**, 521 (1991).
[11] *Dimensions and Entropies in Chaotic Systems*, edited by G. Mayer-Kress (Springer-Verlag, Berlin, 1986).
[12] J. Holzfuss and G. Mayer-Kress, in *Dimensions and Entropies in Chaotic Systems* (Ref. [11]).
[13] A. Branstater and H. L. Swinney, Phys. Rev. A **35**, 2207 (1987).
[14] U. Hübner, W. Klische, N. B. Abraham, and C. O. Weiss, in *Measures of Complexity and Chaos*, edited by N. B. Abraham *et al.* (Plenum, New York, 1990).
[15] K. R. Sreenivasan, in *Dimensions and Entropies in Chaotic Systems* (Ref. [11]).
[16] A. A. Tsonis and J. B. Elsner, Nature (London) **333**, 545 (1988).
[17] D. V. Vassiliadis, A. S. Sharma, T. T. Eastman, and K. Papadopoulos, Geophys. Res. Lett. **17**, 1841 (1990).
[18] A. Ben-Mizrachi, I. Procaccia, and P. Grassberger, Phys. Rev. A **29**, 975 (1984).
[19] J. G. Caputo, in *Measures of Complexity and Chaos*, edited by N. B. Abraham *et al.* (Plenum, New York, 1989).
[20] J. G. Caputo, B. Malraison, and P. Atten, in *Dimensions and Entropies in Chaotic Systems* (Ref. [11]).
[21] J.-P. Eckmann and D. Ruelle, Physica (Amsterdam) **56D**, 185 (1992).
[22] N. A. Gershenfeld, Physica (Amsterdam) **55D**, 155 (1992).
[23] J. W. Havstad and C. L. Ehlers, Phys. Rev. A **39**, 845 (1989).
[24] M. Möller, W. Lange, F. Mischke, N. B. Abraham, and U. Hübner, Phys. Lett. A **138**, 176 (1989).
[25] A. R. Osborne and A. Provenzale, Physica (Amsterdam) **35D**, 357 (1989).
[26] M. C. Mackey and L. Glass, Science **197**, 287 (1977).
[27] P. Grassberger and I. Procaccia, Phys. Rev. A **28**, 2591 (1983); Physica (Amsterdam) **13D**, 34 (1984).
[28] L. A. Smith, Phys. Lett. A **133**, 283 (1988).
[29] The tent map is defined as $y_{n+1} = T(y_n)$, where $T(y) = 2y$ if $0 \leq y < 1/2$ and $T(y) = 2-2y$ if $1/2 \leq y \leq 1$.

KJ

AMERICAN ASSOCIATION FOR THE ADVANCEMENT OF SCIENCE

SCIENCE

30 OCTOBER 1987 $2.50
VOL. 238 ■ PAGES 585–718

Chaos, Strange Attractors, and Fractal Basin Boundaries in Nonlinear Dynamics

CELSO GREBOGI, EDWARD OTT, JAMES A. YORKE

Recently research has shown that many simple nonlinear deterministic systems can behave in an apparently unpredictable and chaotic manner. This realization has broad implications for many fields of science. Basic developments in the field of chaotic dynamics of dissipative systems are reviewed in this article. Topics covered include strange attractors, how chaos comes about with variation of a system parameter, universality, fractal basin boundaries and their effect on predictability, and applications to physical systems.

IN THIS ARTICLE WE PRESENT A REVIEW OF THE FIELD OF chaotic dynamics of dissipative systems including recent developments. The existence of chaotic dynamics has been discussed in the mathematical literature for many decades with important contributions by Poincaré, Birkhoff, Cartwright and Littlewood, Levinson, Smale, and Kolmogorov and his students, among others. Nevertheless, it is only recently that the wide-ranging impact of chaos has been recognized. Consequently, the field is now undergoing explosive growth, and many applications have been made across a broad spectrum of scientific disciplines—ecology, economics, physics, chemistry, engineering, fluid mechanics, to name several. Specific examples of chaotic time dependence include convection of a fluid heated from below, simple models for the yearly variation of insect populations, stirred chemical reactor systems, and the determination of limits on the length of reliable weather forecasting. It is our belief that the number of these applications will continue to grow.

We start with some basic definitions of terms used in the rest of the article.

Dissipative system. In Hamiltonian (conservative) systems such as arise in Newtonian mechanics of particles (without friction), phase space volumes are preserved by the time evolution. (The phase space is the space of variables that specify the state of the system.) Consider, for example, a two-dimensional phase space (q, p), where q denotes a position variable and p a momentum variable. Hamilton's equations of motion take the set of initial conditions at time $t = t_0$ and evolve them in time to the set at time $t = t_1$. Although the shapes of the sets are different, their areas are the same. By a dissipative system we mean one that does not have this property (and cannot be made to have this property by a change of variables). Areas should typically decrease (dissipate) in time so that the area of the final set would be less than the area of the initial set. As a consequence of this, dissipative systems typically are characterized by the presence of attractors.

Attractor. If one considers a system and its phase space, then the initial conditions may be attracted to some subset of the phase space (the attractor) as time $t \to \infty$. For example, for a damped harmonic oscillator (Fig. 1a) the attractor is the point at rest (in this case the origin). For a periodically driven oscillator in its limit cycle the limit set is a closed curve in the phase space (Fig. 1b).

Strange attractor. In the above two examples, the attractors were a point (Fig. 1a), which is a set of dimension zero, and a closed curve (Fig. 1b), which is a set of dimension one. For many other attractors the attracting set can be much more irregular (some would say pathological) and, in fact, can have a dimension that is not an integer. Such sets have been called "fractal" and, when they are attractors, they are called strange attractors. [For a more precise definition see (*1*).] The existence of a strange attractor in a physically interesting model was first demonstrated by Lorenz (*2*).

Dimension. There are many definitions of the dimension d (*3*). The simplest is called the box-counting or capacity dimension and is defined as follows:

$$d = \lim_{\epsilon \to 0} \frac{\ln N(\epsilon)}{\ln(1/\epsilon)} \qquad (1)$$

where we imagine the attracting set in the phase space to be covered by small D-dimensional cubes of edge length ϵ, with D the dimension of the phase space. $N(\epsilon)$ is the minimum number of such cubes needed to cover the set. For example, for a point attractor (Fig. 1a), $N(\epsilon) = 1$ independent of ϵ, and Eq. 1 yields $d = 0$ (as it should). For a limit cycle attractor, as in Fig. 1b, we have that $N(\epsilon) \sim \ell/\epsilon$, where ℓ is the length of the closed curve in the figure (dotted line); hence, for this case, $d = 1$, by Eq. 1. A less trivial example is illustrated in Fig. 2, in the form of a Cantor set. This set is

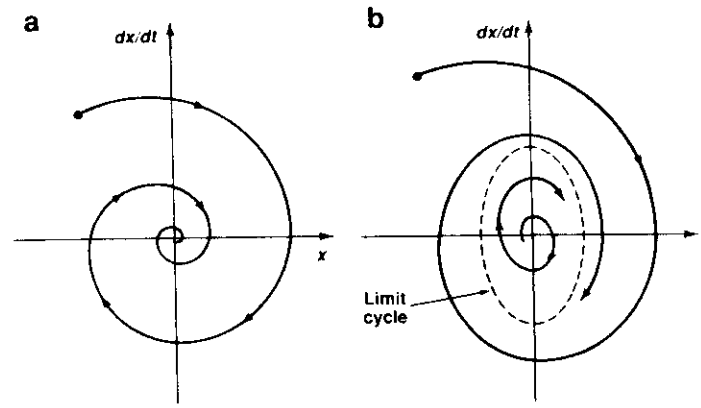

Fig. 1. (**a**) Phase-space diagram for a damped harmonic oscillator. (**b**) Phase-space diagram for a system that is approaching a limit cycle.

C. Grebogi is a research scientist at the Laboratory for Plasma and Fusion Energy Studies. E. Ott is a professor in the departments of electrical engineering and physics, and J. A. Yorke is a professor of mathematics and is the director of the Institute for Physical Science and Technology, University of Maryland, College Park, MD 20742.

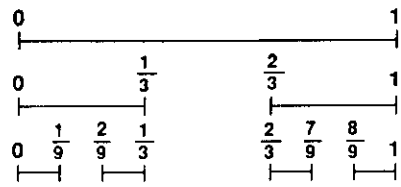

Fig. 2. Construction of a Cantor set.

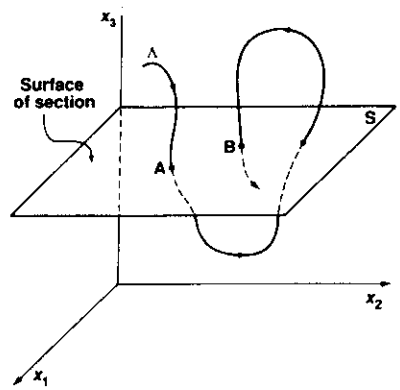

Fig. 3. Poincaré surface of section.

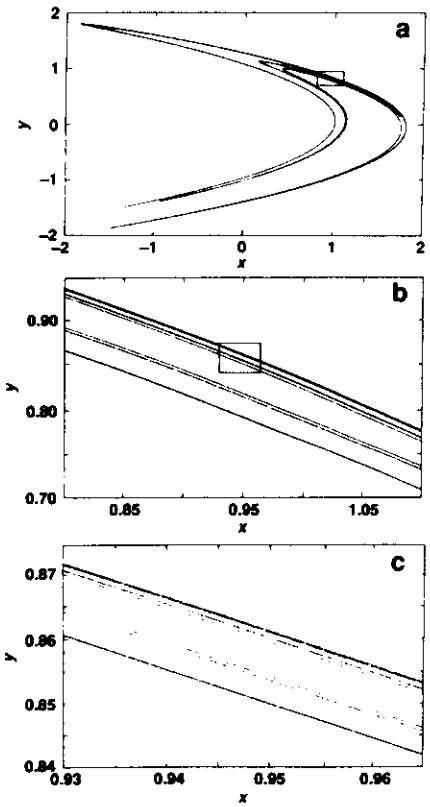

Fig. 4. The Hénon chaotic attractor. (**a**) Full set. (**b**) Enlargement of region defined by the rectangle in (a). (**c**) Enlargement of region defined by the rectangle in (b).

formed by taking the line interval from 0 to 1, dividing it in thirds, then discarding the middle third, then dividing the two remaining thirds into thirds and discarding their middle thirds, and so on ad infinitum. The Cantor set is the closed set of points that are left in the limit of this repeated process. If we take $\epsilon = 3^{-n}$ with n an integer, then we see that $N(\epsilon) = 2^n$ and Eq. 1 (in which $\epsilon \to 0$ corresponds to $n \to \infty$) yields $d = (\ln 2)/(\ln 3)$, a number between 0 and 1, hence, a fractal. The topic of the dimension of strange attractors is a large subject on which much research has been done. One of the most interesting aspects concerning dimension arises from the fact that the distribution of points on a chaotic attractor can be nonuniform in a very singular way. In particular, there can be an arbitrarily fine-scaled interwoven structure of regions where orbit trajectories are dense and sparse. Such attractors have been called multifractals and can be characterized by subsidiary quantities that essentially give the dimensions of the dense and sparse regions of the attractor. In this review we shall not attempt to survey this work. Several papers provide an introduction to recent work on the dimension of chaotic attractors (*3–5*).

Chaotic attractor. By this term we mean that if we take two typical points on the attractor that are separated from each other by a small distance $\Delta(0)$ at $t = 0$, then for increasing t they move apart exponentially fast. That is, in some average sense $\Delta(t) \sim \Delta(0)\exp(ht)$ with $h > 0$ (where h is called the Lyapunov exponent). Thus a small uncertainty in the initial state of the system rapidly leads to inability to forecast its future. [It is not surprising, therefore, that the pioneering work of Lorenz (*2*) was in the context of meteorology.] It is typically the case that strange attractors are also chaotic [although this is not always so; see (*1, 6*)].

Dynamical system. This is a system of equations that allows one, in principle, to predict the future given the past. One example is a system of first-order ordinary differential equations in time, $d\mathbf{x}(t)/dt = \mathbf{G}(\mathbf{x},t)$, where $\mathbf{x}(t)$ is a D-dimensional vector and $\mathbf{G}$ is a D-dimensional vector function of $\mathbf{x}$ and t. Another example is a map.

Map. A map is an equation of the form $\mathbf{x}_{t+1} = \mathbf{F}(\mathbf{x}_t)$, where the "time" t is discrete and integer valued. Thus, given $\mathbf{x}_0$, the map gives $\mathbf{x}_1$. Given $\mathbf{x}_1$, the map gives $\mathbf{x}_2$, and so on. Maps can arise in continuous time physical systems in the form of a Poincaré surface of section. Figure 3 illustrates this. The plane x_3 = constant is the surface of section (S in the figure), and A denotes a trajectory of the system. Every time A pierces S going downward (as at points A and B in the figure), we record the coordinates (x_1,x_2). Clearly the coordinates of A uniquely determine those of B. Thus there exists a map, B = F(A), and this map (if we knew it) could be iterated to find all subsequent piercings of S.

Chaotic Attractors

As an example of a strange attractor consider the map first studied by Hénon (*7*):

$$x_{n+1} = \alpha - x_n^2 + \beta y_n \tag{2}$$

$$y_{n+1} = x_n \tag{3}$$

Figure 4a shows the result of plotting 10^4 successive points obtained by iterating Eqs. 2 and 3 with parameters $\alpha = 1.4$ and $\beta = 0.3$ (and the initial transient is deleted). The result is essentially a picture of the chaotic attractor. Figure 4, b and c, shows successive enlargements of the small square in the preceding figure. Scale invariant, Cantor set–like structure transverse to the linear structure is evident. This suggests that we may regard the attractor in Fig. 4c, for example, as being essentially a Cantor set of approximately straight parallel lines. In fact, the dimension d in Eq. 1 can be estimated numerically (*8*) to be $d \cong 1.26$ so that the attractor is strange.

As another example consider a forced damped pendulum described by the equation

$$d^2\theta/dt^2 + \nu d\theta/dt + \omega_0^2\sin\theta = f\cos(\omega t) \tag{4}$$

where θ is the angle between the pendulum arm and the rest position, ν is the coefficient of friction, ω_0 is the frequency of natural oscillation, and f is the strength of the forcing. In Eq. 4, the first term represents the inertia of the pendulum, the second term represents friction at the pivot, the third represents the gravitational force, and the right side represents an external sinusoidally varying torque of strength f and frequency ω applied to the pendulum at the pivot. In Fig. 5a, we plot the Poincaré surface of section of a strange

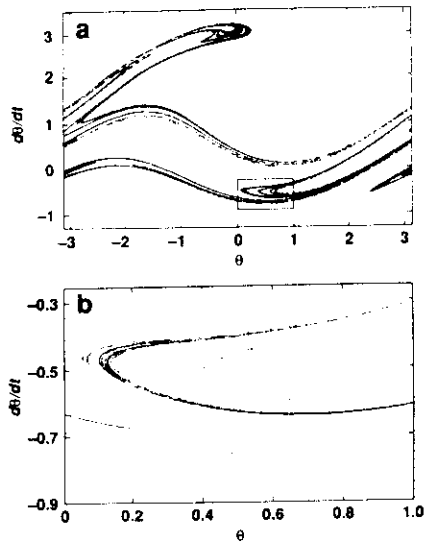

Fig. 5. (**a**) Poincaré surface of section of a pendulum strange attractor. (**b**) Enlargement of region defined by rectangle in (a).

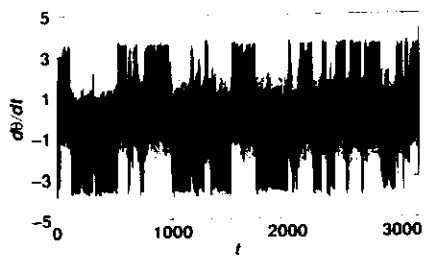

Fig. 6. Chaotic time series for pendulum shown as a plot of angular velocity versus time.

attractor for the pendulum, where we choose $\nu = 0.22$, $\omega_0 = 1.0$, $\omega = 1.0$, and $f = 2.7$ in Eq. 4. This surface of section is obtained by plotting 50,000 dots, one dot for every cycle of the forcing term, that is, one dot at every time $t = t_n = 2\pi n$ (where n is an integer). The strange attractor shown in Fig. 5a exhibits a Cantor set–like structure transverse to the linear structure. This is evident in Fig. 5b, which shows an enlargement of the square region in Fig. 5a. The dimension of this strange attractor in the surface of section is $d \cong 1.38$. Figure 6 shows the angular velocity $d\theta/dt$ as a function of t for the parameters of Fig. 5. Note the apparently erratic nature of this plot.

In general, the form of chaotic attractors varies greatly from system to system and even within the same system. This is indicated by the sequence of chaotic attractors shown in Fig. 7. All of these attractors were generated from the same map (*9*),

$$\psi_{n+1} = [\psi_n + \omega_1 + \epsilon P_1(\psi_n,\theta_n)] \bmod 1 \quad (5)$$

$$\theta_{n+1} = [\theta_n + \omega_2 + \epsilon P_2(\psi_n,\theta_n)] \bmod 1 \quad (6)$$

where P_1 and P_2 are periodic with period one in both their arguments. The P_1 and P_2 are the same in all of the cases shown in Fig. 7; only the parameters ω_1, ω_2, and ϵ have been varied. The results show the great variety of form and structure possible in chaotic attractors as well as their aesthetic appeal. Since ψ and θ may be regarded as angles, Eqs. 5 and 6 are a map on a two-dimensional toroidal surface. [This map is used in (*9*) to study the transition from quasiperiodicity to chaos.]

Because of the exponential divergence of nearby orbits on chaotic attractors, there is a question as to how much of the structure in these pictures of chaotic attractors (Figs. 4, 5, and 7) is an artifact due to chaos-amplified roundoff error. Although a numerical trajectory will diverge rapidly from the true trajectory with the same initial point, it has been demonstrated rigorously (*10*) in important cases [including the Hénon map (*11*)] that there exists a true trajectory with a slightly different initial point that stays near the noisy trajectory for a long time. [For example, for the Hénon map for a typical numerical trajectory computed with 14-digit precision there exists a true trajectory that stays within 10^{-7} of the numerical trajectory for 10^7 iterates (*11*).] Thus we believe that the apparently fractal structure seen in pictures such as Figs. 4, 5, and 7 is real.

The Evolution of Chaotic Attractors

In dissipative dynamics it is common to find that for some value of a system parameter only a nonchaotic attracting orbit (a limit cycle, for example) occurs, whereas at some other value of the parameter a chaotic attractor occurs. It is therefore natural to ask how the one comes about from the other as the system parameter is varied continuously. This is a fundamental question that has elicited a great deal of attention (*9*, *12–19*).

To understand the nature of this question and some of the possible answers to it, we consider Fig. 8a, the so-called bifurcation diagram for the map.

$$x_{n+1} = C - x_n^2 \quad (7)$$

where C is a constant. Figure 8a can be constructed as follows: take $C = -0.4$, set $x_0 = -0.5$, iterate the map 100 times (to eliminate transients), then plot the next 1000 values of x; increase C by a small amount, say 0.001, and repeat what was done for $C = -0.4$; increase again, and repeat; and so on, until $C = 2.1$ is reached. We see from Fig. 8a that below a certain value, $C = C_0 = -0.25$, there is no attractor in $-2 < x < 2$. In fact, in this case all orbits go to $x \to -\infty$, hence the absence of points on the plot. This is also true for C above the "crisis value" $C_c = 2.0$. Between these two values there is an attractor. As C is increased we have an attracting orbit of "period one," which, at $C = 0.75$, bifurcates to a period-two attracting orbit ($x_\alpha \to x_\beta \to x_\alpha \to x_\beta \to \cdots$), which then bifurcates (at $C = 1.25$) to a period-four orbit ($x_a \to x_b \to x_c \to x_d \to x_a \to x_b \to x_c \to x_d \to x_a \to \cdots$). In fact, there are an infinite number of such bifurcations of period 2^n to period 2^{n+1} orbits, and these accumulate as $n \to \infty$ at a finite value of C, which we denote C_∞ (from Fig. 8a, $C_\infty \cong 1.4$). [The practical importance of this phenomenology was emphasized early on by May (*12*).]

What is the situation for $C_\infty < C < C_c$? Numerically what one sees is that for many C values in this range the orbits appear to be chaotic, whereas for others there are periodic orbits. For example, Fig. 8b shows an enlargement of Fig. 8a for C in the range $1.72 < C < 1.82$. We see what appear to be chaotic orbits below $C = C_0^{(3)} = 1.75$. However, just above this value, a period-three orbit appears, supplanting the chaos. The period-three orbit then goes through a period-doubling cascade, becomes chaotic, widens into a three-piece chaotic attractor, and then finally at $C = C_c^{(3)} \cong 1.79$ widens back into a single chaotic band. We call the region $C_0^{(3)} < C < C_c^{(3)}$ a period-three window. (Such windows, but of higher period, appear throughout the region $C_\infty < C < C_c$, but are not as discernible in Fig. 8a because they are much narrower than the period-three window.)

An infinite period-doubling cascade is one way that a chaotic attractor can come about from a nonchaotic one (*13*). There are also two other possible routes to chaos exemplified in Fig. 8, a and b. These are the intermittency route (*14*) and the crisis route (*15*).

Intermittency. Consider Fig. 8b. For C just above $C_0^{(3)}$ there is a period-three orbit. For C just below $C_0^{(3)}$ there appears to be a chaotic orbit. To understand the character of this transition it is useful to examine the chaotic orbit for C just below $C_0^{(3)}$. The character of this orbit is as follows: The orbit appears to be a period-three orbit for long stretches of time after which there is a short

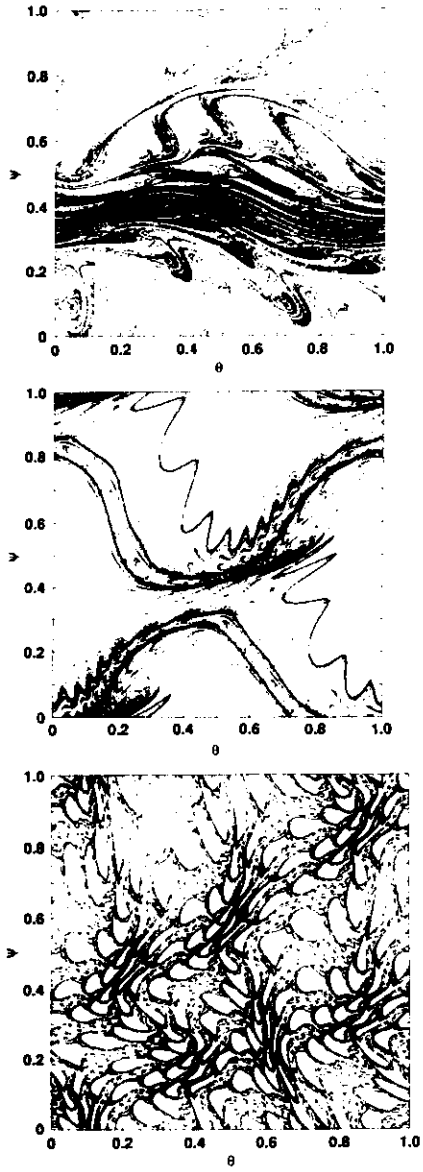

Fig. 7. Sequence of chaotic attractors for system represented by Eqs. 5 and 6. Plot shows iterated mapping on a torus for different values of ω_1, ω_2, and ϵ. (**Top**) $\omega_1 = 0.54657$, $\omega_2 = 0.36736$, and $\epsilon = 0.75$. (**Center**) $\omega_1 = 0.45922$, $\omega_2 = 0.53968$, and $\epsilon = 0.50$. (**Bottom**) $\omega_1 = 0.41500$, $\omega_2 = 0.73500$, and $\epsilon = 0.60$.

burst (the "intermittent burst") of chaotic-like behavior, followed by another long stretch of almost period-three behavior, followed by a chaotic burst, and so on. As C approaches $C_0^{(3)}$ from below, the average duration of the long stretches between the intermittent bursts becomes longer and longer (*14*), approaching infinity and proportional to $(C_0^{(3)} - C)^{-1/2}$ as $C \to C_0^{(3)}$. Thus the pure period-three orbit appears at $C = C_0^{(3)}$. Alternatively we may say that the attracting periodic attractor of period three is converted to a chaotic attractor as the parameter C decreases through the critical value $C_0^{(3)}$. It should be emphasized that, although our illustration of the transition to chaos by way of intermittency is within the context of the period-three window of the quadratic map given by Eq. 7, this phenomenon (as well as period-doubling cascades and crises) is very general; in other systems it occurs for other periods (period one, for example) in easily observable form.

Crises. From Fig. 8a we see that there is a chaotic attractor for $C < C_c = 2$, but no chaotic attractor for $C > C_c$. Thus, as C is lowered through C_c, a chaotic attractor is born. How does this occur? Note that at $C = C_c$ the chaotic orbit occupies the interval $-2 \le x \le 2$. If C is just slightly larger than C_c, an orbit with initial condition in the interval $-2 < x < 2$ will typically follow a chaotic-like path for a finite time, after which it finds its way out of the interval $-2 \le x \le 2$, and then rapidly begins to move to large negative x values (that is, it begins to approach $x = -\infty$). This is called a chaotic transient (*15*). The length of a chaotic transient will depend on the particular initial condition chosen. One can define a mean transient duration by averaging over, for example, a uniform distribution of initial conditions in the interval $-2 < x < 2$. For the quadratic map, this average duration is

$$\tau \sim 1/(C - C_c)^{\gamma} \tag{8}$$

with the exponent γ given by $\gamma = 1/2$. Thus as C approaches C_c from above, the lifetime of a chaotic transient goes to infinity and the transient is converted to a chaotic attractor for $C < C_c$. Again, this type of phenomenon occurs widely in chaotic systems. For example, the model of Lorenz (*2*) for the nonlinear evolution of the Rayleigh-Bénard instability of a fluid subjected to gravity and heated from below has a chaotic onset of the crisis type and an accompanying chaotic transient. In that case, γ in Eq. 8 is $\gamma \sim 4$ (*20*). In addition, a theory for determining the exponent γ for two-dimensional maps and systems such as the forced damped pendulum has recently been published (*21*). Thus we have seen that the period doubling, intermittency, and crisis routes to chaos are illustrated by the simple quadratic map (Eq. 7).

We emphasize that, although a map was used for illustrating these routes, all of these phenomena are present in continuous-time systems and have been observed in experiments. As an example of chaotic transitions in a continuous time system, we consider the set of three autonomous ordinary differential equations studied by Lorenz (*2*) as a model of the Rayleigh-Bénard instability,

$$dx/dt = Py - Px \tag{9}$$

$$dy/dt = -xz + rx - y \tag{10}$$

$$dz/dt = xy - bz \tag{11}$$

where P and b are adjustable parameters. Fixing $P = 10$ and $b = 8/3$ and varying the remaining parameter, r, we obtain numerical solutions that are clear examples of the intermittency and crisis types of chaotic transitions discussed above. We illustrate these in Fig. 9, a through d; the behavior of this system is as follows:

1) For r between 166.0 and 166.2 there is an intermittency transition from a periodic attractor ($r = 166.0$, Fig. 9a) to a chaotic attractor ($r = 166.2$, Fig. 9b) with intermittent turbulent bursts. Between the bursts there are long stretches of time for which the orbit oscillates in nearly the same way as for the periodic attractor (*14*) (Fig. 9a).

2) For a range of r values below $r = 24.06$ there are two periodic attractors, that represent clockwise and counterclockwise convections. For r slightly above 24.06, however, there are three attractors, one that is chaotic (shown in the phase space trajectory in Fig. 9c), whereas the other two attractors are the previously mentioned periodic attractors. The chaotic attractor comes into existence as r increases through $r = 24.06$ by conversion of a chaotic transient. Figure 9d shows an orbit in phase space executing a chaotic transient before settling down to its final resting place at one of the periodic attractors. Note the similarity of the chaotic transient trajectory in Fig. 9d with the chaotic trajectory in Fig. 9c.

The various routes to chaos have also received exhaustive experimental support. For instance, period-doubling cascades have been observed in the Rayleigh-Bénard convection (*22, 23*), in nonlinear circuits (*24*), and in lasers (*25*); intermittency has been observed in the Rayleigh-Bénard convection (*26*) and in the Belousov-Zhabotinsky reaction (*27*); and crises have been observed in nonlinear circuits (*28–30*), in the Josephson junction (*31*), and in lasers (*32*).

Finally, we note that period doubling, intermittency, and crises do not exhaust the possible list of routes to chaos. (Indeed, the

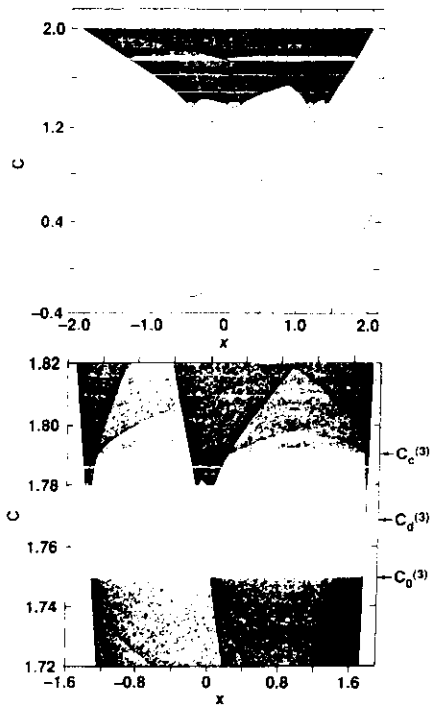

Fig. 8. (**Top**) Bifurcation diagram for the quadratic map. (**Bottom**) Period-three window for the quadratic map.

routes are not all known.) In particular, chaotic onsets involving quasiperiodicity have not been discussed here (*9*, *16*, *18*).

Universality

Universality refers to the fact that systems behave in certain quantitative ways that depend not on the detailed physics or model description but rather only on some general properties of the system. Universality has been examined by renormalization group (*33*) techniques developed for the study of critical phenomena in condensed matter physics. In the context of dynamics, Feigenbaum (*13*) was the first to apply these ideas, and he has extensively developed them, particularly for period doubling for dissipative systems. [See (*17*) for a collection of papers on universality in nonlinear dynamics.] For period doubling in dissipative systems, results have been obtained on the scaling behavior of power spectra for time series of the dynamical process (*34*), on the effect of noise on period doubling (*35*), and on the dependence of the Lyapunov exponent (*36*) on a system parameter. Applications of the renormalization group have also been made to intermittency (*19*, *37*), and the breakdown of quasiperiodicity in dissipative (*18*) and conservative (*38*) systems.

As examples, two "universal" results can be stated within the context of the bifurcation diagrams (Fig. 8, a and b). Let C_n denote the value of C at which a period 2^n cycle period doubles to become a period 2^{n+1} cycle. Then, for the bifurcation diagram in Fig. 8a, one obtains

$$\lim_{n\to\infty} \frac{C_n - C_{n-1}}{C_{n+1} - C_n} = 4.669201\ldots \qquad (12)$$

The result given in Eq. 12 is not restricted to the quadratic map. In fact, it applies to a broad class of systems that undergo period doubling cascades (*13*, *39*). In practice such cascades are very common, and the associated universal numbers are observed to be well approximated by means of fairly low order bifurcations (for example, n = 2,3,4). This scaling behavior has been observed in many experiments, including ones on fluids, nonlinear circuits, laser systems, and so forth. Although universality arguments do not explain why cascades must exist, such explanations are available from bifurcation theory (*40*).

Figure 8b shows the period-three window within the chaotic range of the quadratic map. As already mentioned, there are an infinite number of such periodic windows. [In fact, they are generally believed to be dense in the chaotic range. For example, if k is prime, there are $(2^k - 2)/(2k)$ period-k windows.] Let $C_0^{(k)}$ and $C_c^{(k)}$ denote the upper and lower values of C bounding the period-k window and let $C_d^{(k)}$ denote the value of C at which the period-k attractor bifurcates to period $2k$. Then we have that, for typical k windows (*41*).

$$\lim_{k\to\infty} \frac{C_c^{(k)} - C_0^{(k)}}{C_d^{(k)} - C_0^{(k)}} \to 9/4 \qquad (13)$$

In fact, even for the k = 3 window (Fig. 8b) the 9/4 value is closely approximated (it is 9/4 − 0.074 . . .). This result is universal for one-dimensional maps (and possibly more generally for any chaotic dynamical process) with windows.

Fractal Basin Boundaries

In addition to chaotic attractors, there can be sets in phase space on which orbits are chaotic but for which points near the set move away from the set. That is, they are repelled. Nevertheless, such chaotic repellers can still have important macroscopically observable effects, and we consider one such effect (*42*, *43*) in this section.

Typical nonlinear dynamical systems may have more than one time-asymptotic final state (attractor), and it is important to consider the extent to which uncertainty in initial conditions leads to uncertainty in the final state. Consider the simple two-dimensional phase space diagram schematically depicted in Fig. 10. There are two attractors denoted A and B. Initial conditions on one side of the boundary, Σ, eventually asymptotically approach B; those on the other side of Σ eventually go to A. The region to the left or right of Σ is the basin of attraction for attractor A or B, respectively, and Σ is the basin boundary. If the initial conditions are uncertain by an amount ϵ, then for those initial conditions within ϵ of the boundary we cannot say a priori to which attractor the orbit eventually tends.

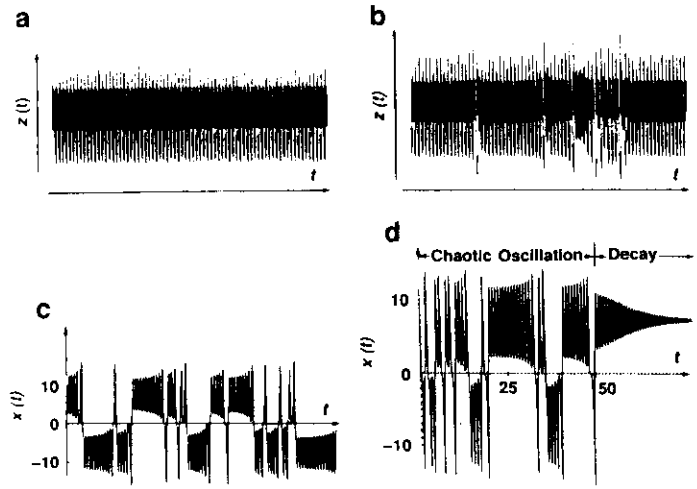

Fig. 9. Intermittency, crisis, and period doubling in continuous time systems. Intermittency in the Lorenz equations (**a**) r = 166.0; (**b**) r = 166.2. Crisis transition to a chaotic attractor in the Lorenz equations: (**c**) r = 28; (**d**) r = 22.

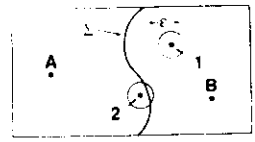

Fig. 10. A region of phase space divided by the basin boundary Σ into basins of attraction for the two attractors A and B. Points 1 and 2 are initial conditions with error ϵ.

For example, in Fig. 10, points 1 and 2 are initial conditions with an uncertainty ϵ. The orbit generated by initial condition 1 is attracted to attractor B. Initial condition 2, however, is uncertain in the sense that the orbit generated by 2 may be attracted either to A or B. In particular, consider the fraction of the uncertain phase space volume within the rectangle shown and denote this fraction f. For the case shown in Fig. 10, we clearly have $f \sim \epsilon$. The main point we wish to make in what follows is that, from the point of view of prediction, much worse scalings of f with ϵ frequently occur in nonlinear dynamics. Namely, the fraction can scale as

$$f \sim \epsilon^{\alpha} \tag{14}$$

with the "uncertainty exponent" α satisfying $\alpha < 1$ (*42, 43*). In fact, $\alpha << 1$ is fairly common. In such a case, a substantial reduction in the initial condition uncertainty, ϵ, yields only a relatively small decrease in the uncertainty of the final state as measured by f.

Although α is equal to unity for simple basin boundaries, such as that depicted in Fig. 10, boundaries with noninteger (fractal) dimension also occur. We use here the capacity definition of dimension, Eq. 1. In general, since the basin boundary divides the phase space, its dimension d must satisfy $d \geq D - 1$, where D is the dimension of the phase space. It can be proven that the following relation between the index α and the basin boundary dimension holds (*42, 43*)

$$\alpha = D - d \tag{15}$$

For a simple boundary, such as that depicted in Fig. 10, we have $d = D - 1$, and Eq. 15 then gives $\alpha = 1$, as expected. For a fractal basin boundary, $d > D - 1$, and Eq. 15 gives $\alpha < 1$.

We now illustrate the above with a concrete example. Consider the forced damped pendulum as given by Eq. 4. For parameter values $\nu = 0.2$, $\omega_0 = 1.0$, $\omega = 1.0$, and $f = 2.0$, we find numerically that the only attractors in the surface of section (θ, $d\theta/dt$) are the fixed points $(-0.477, -0.609)$ and $(-0.471, 2.037)$. They represent solutions with average counterclockwise and clockwise rotation at the period of the forcing. The cover shows a computer-generated picture of the basins of attraction for the two fixed point attractors. Each initial condition in a 1024 by 1024 point grid is integrated until it is close to one of the two attractors (typically 100 cycles). If an orbit goes to the attractor at $\theta = -0.477$, a blue dot is plotted at the corresponding initial condition. If the orbit goes to the other attractor, a red dot is plotted. Thus the blue and red regions are essentially pictures of the basins of attraction for the two attractors to the accuracy of the grid of the computer plotter. Fine-scale structure in the basins of attraction is evident. This is a consequence of the Cantor-set nature of the basin boundary. In fact, magnifications of the basin boundary show that, as we examine it on a smaller and smaller scale, it continues to have structure.

We now wish to explore the consequences for prediction of this infinitely fine-scaled structure. To do this, consider an initial condition (θ, $d\theta/dt$). What is the effect of a small change ϵ in the θ-coordinate? Thus we integrate the forced pendulum equation with the initial conditions (θ, $d\theta/dt$), (θ, $d\theta/dt + \epsilon$), and (θ, $d\theta/dt - \epsilon$) until they approach one of the attractors. If either or both of the perturbed initial conditions yield orbits that do not approach the same attractor as the unperturbed initial condition, we say that (θ, $d\theta/dt$) is uncertain. Now we randomly choose a large number of initial conditions and let $\hat{f}$ denote the fraction of these that we find to be uncertain. As a result of these calculations, we find that $\hat{f} \sim \epsilon^{\hat{\alpha}}$ where $\hat{\alpha} \cong 0.275 \pm 0.005$. If we assume that $\hat{f}$, determined in the way stated above, is approximately proportional to f [there is some support for this conjecture from theoretical work (*44*)], then $\alpha = \hat{\alpha}$. Thus, from Eq. 15, the dimension of the basin boundary is $d \cong 1.725 \pm 0.005$. We conclude, from Eq. 14, that in this case if we are to gain a factor of 2 in the ability to predict the asymptotic final state of the system, it is necessary to increase the accuracy in the measurement of the initial conditions by a factor substantially greater than 2 (namely by $2^{1/0.275} \cong 10$). Hence, fractal basin boundaries ($\alpha < 1$) represent an obstruction to predictability in nonlinear dynamics.

Some representative works on fractal basin boundaries, including applications, are listed in (*42–47*). Notable basic questions that have recently been answered are the following:

1) How does a nonfractal basin boundary become a fractal basin boundary as a parameter of the system is varied (*45*)? This question is similar, in spirit, to the question of how chaotic attractors come about.

2) Can fractal basin boundaries have different dimension values in different regions of the boundary, and what boundary structures lead to this situation? This question is addressed in (*46*) where it is shown that regions of different dimension can be intertwined on an arbitrarily fine scale.

3) What are the effects of a fractal basin boundary when the system is subject to noise? This has been addressed in the Josephson junction experiments of (*31*).

Conclusion

Chaotic nonlinear dynamics is a vigorous, rapidly expanding field. Many important future applications are to be expected in a variety of areas. In addition to its practical aspects, the field also has fundamental implications. According to Laplace, determination of the future depends only on the present state. Chaos adds a basic new aspect to this rule: small errors in our knowledge can grow exponentially with time, thus making the long-term prediction of the future impossible.

Although the field has advanced at a great rate in recent years, there is still a wealth of challenging fundamental questions that have yet to be adequately dealt with. For example, most concepts developed so far have been discovered in what are effectively low-dimensional systems; what undiscovered important phenomena will appear only in higher dimensions? Why are transiently chaotic motions so prevalent in higher dimensions? In what ways is it possible to use the dimension of a chaotic attractor to determine the dimension of the phase space necessary to describe the dynamics? Can renormalization group techniques be extended past the borderline of chaos into the strongly chaotic regime? These are only a few questions. There are many more, and probably the most important questions are those that have not yet been asked.

REFERENCES AND NOTES

1. C. Grebogi, E. Ott, S. Pelikan, J. A. Yorke, *Physica* **13D**, 261 (1984).
2. E. N. Lorenz, *J. Atmos. Sci.* **20**, 130 (1963).
3. J. D. Farmer, E. Ott, J. A. Yorke, *Physica* **7D**, 153 (1983).
4. J. Kaplan and J. A. Yorke, *Lecture Notes in Mathematics No. 730* (Springer-Verlag, Berlin, 1978), p. 228; L. S. Young, *Ergodic Theory Dyn. Syst.* **1**, 381 (1981).
5. P. Grassberger and I. Procaccia, *Phys. Rev. Lett.* **50**, 346 (1983); H. G. E. Hentschel and I. Procaccia, *Physica* **8D**, 435 (1983); P. Grassberger, *Phys. Lett.* **A97**, 227 (1983); T. C. Halsey *et al.*, B. I. Shraiman, *Phys. Rev. A* **33**, 1141 (1986); C. Grebogi, E. Ott, J. A. Yorke, *ibid.* **36**, 3522 (1987).
6. A. Bondeson *et al.*, *Phys. Rev. Lett.* **55**, 2103 (1985); F. J. Romeiras, A. Bondeson, E. Ott, T. M. Antonsen, C. Grebogi, *Physica* **26D**, 277 (1987).
7. M. Hénon, *Commun. Math. Phys.* **50**, 69 (1976).
8. D. A. Russell, J. D. Hanson, E. Ott, *Phys. Rev. Lett.* **45**, 1175 (1980).
9. C. Grebogi, E. Ott, J. A. Yorke, *Physica* **15D**, 354 (1985).

10. D. V. Anosov, *Proc. Steklov Ins. Math.* **90** (1967); R. Bowen, *J. Differ. Equations* **18**, 333 (1975).
11. S. M. Hammel, J. A. Yorke, C. Grebogi, *J. Complexity*, **3**, 136 (1987).
12. R. M. May, *Nature (London)* **261**, 459 (1976).
13. M. J. Feigenbaum, *J. Stat. Phys.* **19**, 25 (1978).
14. Y. Pomeau and P. Manneville, *Commun. Math. Phys.* **74**, 189 (1980).
15. C. Grebogi, E. Ott, J. A. Yorke, *Physica* **7D**, 181 (1983).
16. D. Ruelle and F. Takens, *Commun. Math. Phys.* **20**, 167 (1971).
17. P. Cvitanovic, Ed. *Universality in Chaos* (Hilger, Bristol, 1984).
18. For example, S. J. Shenker, *Physica* **5D**, 405 (1982); K. Kaneko, *Progr. Theor. Phys.* 71, 282 (1984); M. J. Feigenbaum, L. P. Kadanoff, S. L. Shenker, *Physica* **8D**, 303 (1983); S. Kim and S. Ostlund, *Phys. Rev. Lett.* **55**, 1165 (1985); D. K. Umberger, J. D. Farmer, I. J. Satija, *Phys. Lett. A* **114**, 341 (1986); P. Bak, T. Bohr, M. H. Jensen, *Phys. Scr.* **T9**, 50 (1985); P. Bak, *Phys. Today* **39** (No. 12), 38 (1987).
19. J. E. Hirsch, M. Nauenberg, D. J. Scalapino, *Phys. Lett. A* **87**, 391 (1982).
20. J. A. Yorke and E. D. Yorke, *J. Stat. Phys.* **21**, 263 (1979); in *Topics in Applied Physics* (Springer-Verlag, New York, 1981), vol. 45, p. 77.
21. C. Grebogi, E. Ott, J. A. Yorke, *Phys. Rev. Lett.* **57**, 1284 (1986).
22. A. Libchaber and J. Maurer, *J. Phys. (Paris)* **41**, C3-51 (1980); A. Libchaber, C. Laroche, S. Fauve, *J. Phys. (Paris) Lett.* **43**, L211 (1982).
23. J. P. Gollub, S. V. Benson, J. F. Steinman, *Ann. N.Y. Acad. Sci.* **357**, 22 (1980); M. Giglio, S. Musazzi, U. Perini, *Phys. Rev. Lett.* **47**, 243 (1981).
24. P. S. Linsay, *Phys. Rev. Lett.* **47**, 1349 (1981).
25. F. T. Arecchi, R. Meucci, G. Puccioni, J. Tredicce, *ibid.* **49**, 1217 (1982).
26. M. Dubois, M. A. Rubio, P. Bergé, *ibid.* **51**, 1446 (1983).
27. J. C. Roux, P. DeKepper, H. L. Swinney, *Physica* **7D**, 57 (1983).
28. C. Jeffries and J. Perez, *Phys. Rev. A* **27**, 601 (1983); S. K. Brorson, D. Dewey, P. S. Linsay, *ibid.* **28**, 1201 (1983).
29. H. Ikezi, J. S. deGrasse, T. H. Jensen, *ibid.* **28**, 1207 (1983).
30. R. W. Rollins and E. R. Hunt, *ibid.* **29**, 3327 (1984).
31. M. Iansiti *et al.*, *Phys. Rev. Lett.* **55**, 746 (1985).
32. D. Dangoisse, P. Glorieux, D. Hannequin, *ibid.* **57**, 2657 (1986).
33. K. G. Wilson and J. Kogut, *Phys. Rep. C* **12**, 75 (1974); B. Hu, *ibid.* **91**, 233 (1982).
34. M. J. Feigenbaum, *Phys. Lett. A* **74**, 375 (1979); R. Brown, C. Grebogi, E. Ott, *Phys. Rev. A* **34**, 2248 (1986); M. Nauenberg and J. Rudnick, *Phys. Rev. B* **24**, 493 (1981); B. A. Huberman and A. B. Zisook, *Phys. Rev. Lett.* **46**, 626 (1981); J. D. Farmer, *ibid.* **47**, 179 (1981).
35. J. Crutchfield, M. Nauenberg, J. Rudnick, *Phys. Rev. Lett.* **46**, 933 (1981); B. Shraiman, C. E. Wayne, P. C. Martin, *ibid.*, p. 935.
36. B. A. Huberman and J. Rudnick, *ibid.* **45**, 154 (1980).
37. B. Hu and J. Rudnick, *ibid.* **48**, 1645 (1982).
38. L. P. Kadanoff, *ibid.* **47**, 1641 (1981); D. F. Escande and F. Doveil, *J. Stat. Phys.* 26, 257 (1981); R. S. MacKay, *Physica* **7D**, 283 (1983).
39. P. Collet, J. P. Eckmann, O. E. Lanford III, *Commun. Math. Phys.* 76, 211 (1980).
40. J. A. Yorke and K. A. Alligood, *ibid.* **100**, 1 (1985).
41. J. A. Yorke, C. Grebogi, E. Ott, L. Tedeschini-Lalli, *Phys. Rev. Lett.* **54**, 1095 (1985).
42. C. Grebogi, S. W. McDonald, E. Ott, J. A. Yorke, *Phys. Lett. A* **99**, 415 (1983).
43. S. W. McDonald, C. Grebogi, E. Ott, J. A. Yorke, *Physica* **17D**, 125 (1985).
44. S. Pelikan, *Trans. Am. Math. Soc.* **292**, 695 (1985).
45. C. Grebogi, E. Ott, J. A. Yorke, *Phys. Rev. Lett.* **56**, 1011 (1986); *Physica* **24D**, 243 (1987); F. C. Moon and G.-X. Li, *Phys. Rev. Lett.* **55**, 1439 (1985).
46. C. Grebogi, E. Kostelich, E. Ott, J. A. Yorke, *Phys. Lett.* **A118**, 448 (1986); *Physica* **25D**, 347 (1987); C. Grebogi, E. Ott, J. A. Yorke, H. E. Nusse, *Ann. N.Y. Acad. Sci.* **497**, 117 (1987).
47. C. Mira, *C. R. Acad. Sci.* **288A**, 591 (1979); C. Grebogi, E. Ott, J. A. Yorke, *Phys. Rev. Lett.* **50**, 935 (1983); R. G. Holt and I. B. Schwartz, *Phys. Lett.* **A105**, 327 (1984); I. B. Schwartz, *ibid.* **106**, 339 (1984); I. B. Schwartz, *J. Math. Biol.* **21**, 347 (1985); S. Takesue and K. Kaneko, *Progr. Theor. Phys.* **71**, 35 (1984); O. Decroly and A. Goldbeter, *Phys. Lett.* **A105**, 259 (1984); E. G. Gwinn and R. M. Westervelt, *Phys. Rev. Lett.* **54**, 1613 (1985); *Phys. Rev. A* **33**, 4143 (1986); Y. Yamaguchi and N. Mishima, *Phys. Lett.* **A109**, 196 (1985); M. Napiorkowski, *ibid.* **113**, 111 (1985); F. T. Arecchi, R. Badii, A. Politi, *Phys. Rev. A* **32**, 402 (1985); S. W. McDonald, C. Grebogi, E. Ott, J. A. Yorke, *Phys. Lett.* **A107**, 51 (1985); J. S. Nicolis and I. Tsuda, in *Simulation, Communication, and Control*, S. G. Tzafestas, Ed. (North-Holland, Amsterdam, 1985); J. S. Nicolis, *Rep. Prog. Phys.* **49**, 1109 (1986); J. S. Nicolis, *Kybernetes* **14**, 167 (1985).
48. This work was supported by the Air Force Office of Scientific Research, the U.S. Department of Energy, the Defense Advanced Research Projects Agency, and the Office of Naval Research.

COVER Even systems as simple as a periodically forced damped pendulum can have complex behavior. This computer-generated plot shows initial pendulum velocities (measured horizontally) and positions (measured vertically). Orbits starting at points in the red region eventually settle into one type of periodic motion, while orbits starting in the blue region yield a different type of periodic motion. The boundary between these regions is fractal. The lighter the shade of red or blue, the longer it takes to settle into the corresponding motion. See page 632. [Photo courtesy of C. Grebogi, E. Ott, and J. A. Yorke, University of Maryland, College Park, MD 20742]